

# JULIO: Candidate Engine for a Future Concorde

## AIAA Contest 2020-2021 Undergraduate Engine Design Competition

**Faculty Advisor:** Juan Pablo Alvarado Perilla

**Team Leader:** Danna Yuliza Giraldo Orozco

**Team Members:**

Sebastián Álvarez Zuluaga

Camilo Ramirez Restrepo

Isabella Seguro Muñetón

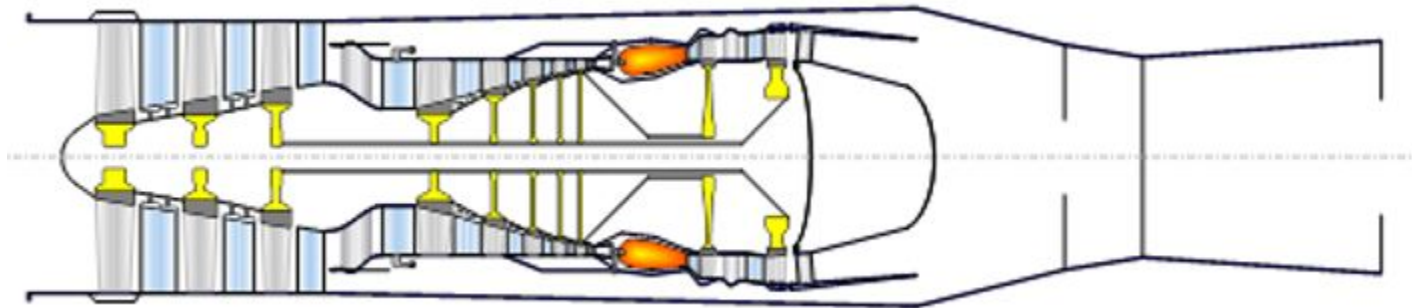
Steven Orlando Silgado Correa

Manuela Sánchez Villa

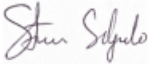
Daniel José Blandón Del Castillo

Juan Fernando Zapata Coronel

David Gonzáles Betancur



## Signature Page

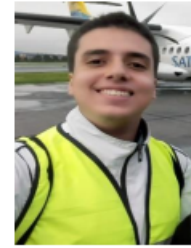
NAME	AIAA MEMBERSHIP	SIGNATURE
Faculty Advisor Juan Pablo Alvarado Perilla	268610	Juan Pablo Alvarado P.
Danna Yuliza Giraldo Orozco	1193405	
Sebastián Álvarez Zuluaga	1193315	Sebastian Alvarez Zuluaga
Camilo Ramirez Restrepo	1194019	Camilo Ramirez Rpo
Isabella Seguro Muñetón	1217661	Isabella Seguro Muñetón
Steven Orlando Silgado Correa	1217355	
Manuela Sánchez Villa	1217535	
Daniel José Blandón del Castillo	1217494	
Juan Fernando Zapata Coronel	1241752	Juan Fernando Z
David González Betancur	1229082	



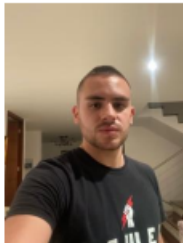
Danna Yuliza Giraldo  
Turbine – Mixer - Nozzle



Sebastián Álvarez Z  
Compressor – Cycle Design



Camilo Ramírez Restrepo  
Compressor – Cycle Design



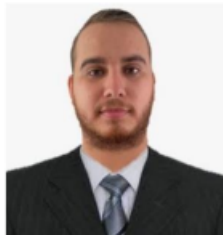
Juan Fernando Zapata C  
Nozzle



Steven O. Silgado Correa  
Combustion Chamber



Isabella Seguro Muñeton  
Combustion Chamber



Daniel José Blandón Del  
Castillo  
Subsystems



Manuela Sanchez Villa  
Subsystems



David González Betancur  
Materials

## **Acknowledgments**

The Kaboom group would like to offer special thanks to:

Juliana Andrea Niño Navia, who is our tutor of the Engine Design group at the Aeronautical Engineering Research of the University. She was always willing to solve our doubts, gave her unconditional support and placed her trust in us.

# Contents

<b>1</b>	<b>Introduction</b>	<b>1</b>
<b>2</b>	<b>Requirements Definitions</b>	<b>2</b>
1	Mission Definition and Thrust requirements . . . . .	2
2	Additional Requirements . . . . .	3
3	Benchmarking . . . . .	3
<b>3</b>	<b>Engine Cycle</b>	<b>3</b>
1	Baseline Engine . . . . .	3
2	Engine Type Definition . . . . .	5
<b>4</b>	<b>Inlet</b>	<b>6</b>
1	Description . . . . .	6
2	Materials and Manufacturing . . . . .	7
<b>5</b>	<b>Compressors</b>	<b>7</b>
1	Fan - Low Pressure Compressor . . . . .	8
1.1	Design Criteria . . . . .	8
1.2	Geometry . . . . .	8
1.3	Fan Design Results . . . . .	9
2	Materials and Manufacturing . . . . .	9
3	High Pressure Compressor . . . . .	10
3.1	Design Criteria . . . . .	10
3.2	Geometry . . . . .	11
4	Materials and Manufacturing . . . . .	12
<b>6</b>	<b>AVC-8015 Combustion Chamber</b>	<b>12</b>
1	Design Point . . . . .	12
2	Type of the combustion . . . . .	13

3	Combustor Design . . . . .	13
3.1	Type of Combustor . . . . .	13
3.2	Diffuser Design . . . . .	14
3.3	Combustor Geometry . . . . .	15
3.4	Burner Pressure Loss . . . . .	17
3.5	Burner Efficiency . . . . .	19
4	Fuel System . . . . .	20
4.1	Fuel Injection . . . . .	20
4.2	Number of Fuel Injectors and Fuel atomizing Flow . . . . .	21
5	Materials and Manufacturing . . . . .	21
6	Cooling or Refrigeration . . . . .	21
7	Ignition . . . . .	24
8	Emissions . . . . .	24
<b>7</b>	<b>Turbine</b>	<b>26</b>
1	High Pressure Turbine . . . . .	26
1.1	Design Criteria . . . . .	26
1.2	Smith Chart and Stages Number . . . . .	27
1.3	Stage Characteristics . . . . .	28
1.4	Velocity Diagram . . . . .	29
1.5	Turbine Blades Cooling . . . . .	29
2	Low Pressure Turbine . . . . .	30
2.1	Design Criteria . . . . .	30
2.2	Smith Chart and Stages Number . . . . .	30
2.3	Stage Characteristics . . . . .	31
2.4	Velocity Diagram . . . . .	31
3	Materials and Manufacturing . . . . .	32
3.1	Blades Materials . . . . .	32

<b>8 Mixer Core-Fan Flow</b>	<b>33</b>
<b>9 Nozzle</b>	<b>34</b>
1 Inlet Conditions . . . . .	34
2 Design Geometry and Area Scheduling . . . . .	34
3 Engine Noise Attenuation . . . . .	36
3.1 Mixer Ejector . . . . .	36
3.2 Chevrons . . . . .	37
<b>10 Shaft</b>	<b>38</b>
<b>11 Engine Subsystems</b>	<b>39</b>
1 Anti – Icing . . . . .	39
2 Bleed Air System . . . . .	39
3 Engine Control System . . . . .	39
4 Starting System . . . . .	40
5 Lubrication System . . . . .	40

## List of Figures

1	Rolls Royce/SNECMA Olympus 593 Gasturb13 engine model. . . . .	4
2	Rolls Royce/SNECMA Olympus 593 modeling results in GasTurb13. . . . .	5
3	Mixed Flow Turbofan Architecture . . . . .	6
4	Fan Operation Map. . . . .	8
5	Fan architecture. . . . .	9
6	High-Pressure Compressor operation map. . . . .	11
7	High-Pressure Compressor architecture. . . . .	12
9	Combined Diffuser Geometry. From [1] . . . . .	14
8	Relative Merits of Various Diffuser Types. From [2] . . . . .	15
10	Combustor Data to obtain the length ratio in Eq. 6.3. From [1] . . . . .	16
11	Combustor Total Pressure Loss. . . . .	19
12	Combustion efficiency correlation. From [3] . . . . .	20
13	Schematic and nomenclature for air partitioning. From [1]. . . . .	22
14	Air Flow $\mu_c$ fraction required for given cooling effectiveness $\Phi$ . From [1]. . . . .	23
15	ICAO CAEP $NO_x$ limits. From [4] . . . . .	26
16	HPT Smith Chart . . . . .	27
17	HPT Velocity Diagram . . . . .	29
18	LPT Smith Chart . . . . .	30
19	LPT Velocity Diagram . . . . .	32
20	Engine Overall Geometry. . . . .	35
21	JT8D-17 20-lobe ejector nozzle showing cruise (left) and takeoff (right) operation. From [5] . . . . .	37
22	Mixer Ejector Model. From [6]. . . . .	37
23	Noise Benefit and Cruise Thrust Loss Data. From [7]. . . . .	38
24	Chevron 3T24C24 Configuration. From [7]. . . . .	38

## List of Tables

1	Concorde General Features. From [8] [9]. . . . .	1
2	Engine Specifications. From [8]. . . . .	2
3	Engine Performance Requirements. From [8]. . . . .	2
4	Bench-marking Engines Considered for Julio Design. From [10]. . . . .	3
5	Engine Comparison Parameters. From [11]. . . . .	5
6	Inlet Flight Conditions. . . . .	6
7	Inlet Geometry Information. . . . .	7
8	Material Properties. . . . .	7
9	Fan Specifications. . . . .	9
10	Material Properties. . . . .	10
11	High-Pressure Compressor Operating Conditions. . . . .	10
12	High-Pressure Compressor design results. . . . .	11
13	Material Properties. . . . .	12
14	Combustor Inlet Condition. . . . .	13
15	Diffuser calculation. . . . .	16
16	Combustor geometry calculation. . . . .	17
17	Combustor Pressure Parameters. . . . .	18
18	Reaction Rate Parameters. . . . .	20
19	Number of Fuel Injectors and Fuel Flow parameters calculation. . . . .	21
20	Required physical properties of Nimonic Alloy 263 <sup>tm</sup> . From [12]. . . . .	21
21	Combustor Air Flow Calculation. . . . .	24
22	Emission Index of $NO_x$ . . . . .	25
23	Emission Mass per unit of Thrust . . . . .	25
24	HPT Parameters Design Reference . . . . .	27
25	HPT Input Stage Data . . . . .	28
26	HPT Output Stage Data . . . . .	28

27	HPT Velocity Values . . . . .	29
28	LPT Parameters Design Reference . . . . .	30
29	LPC Input Stage Data . . . . .	31
30	LPT Output Stage Data . . . . .	31
31	LPT Velocity Values . . . . .	32
32	SiC/SiC Properties. From [13]. . . . .	33
33	Mixer Values . . . . .	34
34	Nozzle inlet conditions . . . . .	34
35	Nozzle Geometry Values . . . . .	35
36	Nozzle Design Results . . . . .	36

## 1. Introduction

A new engine design is required for the Concorde aircraft, which will enter into service in 2028. This aircraft can carry 100 passengers and can reach a speed of Mach 2.0. The most critical phases during its operation are takeoff and cruise, in which JULIO, the proposed engine, will have to comply with the requirements of the RFP [8]. Table 1 shows the general characteristics of the Concorde.

**Table 1 Concorde General Features. From [8] [9].**

<b>Crew</b>	9
<b>Passengers</b>	100
<b>Max. Speed</b>	2.0 M
<b>Max. Range</b>	4500 NM
<b>Endurance</b>	3 h 30 min
<b>Service ceiling</b>	60000 ft
<b>L/D at takeoff</b>	4.0
<b>L/D at cruise</b>	7.4
<b>Max Payload</b>	29500 lbs
<b>Max takeoff Weight</b>	408000 lbs
<b>Max taxing Weight</b>	412000 lbs
<b>Max Landing Weight</b>	245000 lbs
<b>Max Weight of Fuel</b>	210974 lbs
<b>Power Plant</b>	4 x Olympus 593 Mrk610 turbojet with afterburner

Following the RFP guidelines, the Olympus 593 will be the baseline engine as a starting point for the design process. This engine is a turbojet that consists of the inlet, 14 stages of compressors (7 HP and 7 LP), annular combustion chamber, 2 stages of turbines (1 HP and 1 LP), the afterburner that is required during takeoff, and two nozzles with variable geometry, other important engine parameters are specified in the Table 2.

**Table 2 Engine Specifications. From [8].**

<b>Engine Model</b>	Olympus 593 MK 610 Turbojet
<b>Manufacturer</b>	Rolls-Royce/SNECMA
<b>Number of engines</b>	4
<b>Max thrust per engine at takeoff</b>	33620 lbf with afterburner
<b>Max thrust per engine at supersonic cruise</b>	10030 lbf without afterburner
<b>Reheat contribution to performance</b>	20% at full thrust during takeoff
<b>Fuel type</b>	A1 jet fuel
<b>Fuel capacity</b>	210974 lbm
<b>Fuel consumption at full power</b>	23152 lbm
<b>Fuel consumption at full reheat power</b>	49612 lbm
<b>Typical miles/gallon per passenger</b>	17
<b>Engine diameter</b>	47.75 in
<b>Engine length</b>	159 in
<b>Engine length with nozzle</b>	215.34
<b>Engine mass without nozzle</b>	7000 lbm

## **2. Requirements Definitions**

### **A. Mission Definition and Thrust requirements**

For the engine mission, the flight phases defined in the RFP are considered, initially it will have to operate during takeoff with a temperature ISA + 10 °C then it will climb to 40000 ft at a speed of 1.2 Mach and will reach cruise altitude at 53000 ft in which the operating speed is 2.0 Mach. From these conditions the design points are established. The first design point or On Design will be the cruise stage and the Off Design will be the Takeoff phase whose conditions and thrust requirements are shown in the Table 3 .

**Table 3 Engine Performance Requirements. From [8].**

	<b>takeoff</b>	<b>Cruise</b>
<b>Mach Number</b>	0.3	2.0
<b>Altitude [ft]</b>	0	53000
<b>Conditions</b>	ISA + 10 °C	ISA + 5 °C
<b>Inlet Pressure Recovery</b>	0.986	0.937
<b>Afterburner</b>	On	Off
<b>Net thrust [lbf]</b>	33600	10000
<b>SFC</b>	1.39	1.19

## B. Additional Requirements

In addition to achieving the thrust required under the conditions given in Table 3, the new engine must have the following characteristics:

- A low bypass is required as it must be mated into the Concorde structure bearing in mind that the existing inlet is retained.
- Aim for the elimination of the reheat to reduce weight and fuel consumption factors.
- Since this is a transition from turbojet to turbofan, it must be ensured that the increase in diameter is kept to a minimum.
- The temperature limit for the HPT inlet is 3150 °R, for which the use of Carbon Matrix Composites can be considered, justifying the choice of each material. A temperature limit for the HPC outlet of 1620 °R is also established, and in the case of not being able to remove the Reheat, the maximum temperature will be 2100 °R.
- Make the engine optimization, for minimum values of mass and fuel consumption.
- The nozzle configuration must be convergent-divergent with variable geometry and the maximum speed during take-off must not exceed 1150 ft/s to satisfy the noise requirements.

## C. Benchmarking

**Table 4 Bench-marking Engines Considered for Julio Design. From [10].**

Manufacturer	Engine	Thrust (lbf)	OPR	TIT [°C]	Diameter [m]	Weight [kg]	Compressor Stages	Turbine Stages
GE	RR F136	40466	52	-	1.2	-	-	-
PW	F119 (F22)	35969	26.8	-	1.2	1800	6	1HP + 1LP
GE	YF120 (Northrop YF23)	35969	-	-	1.06	1840	5	1HP + 1LP
PW	F100-229 (F15-F16)	29158	32	1350	1.18	1737	10	2HP + 2LP
PW	F135	42939	28	1980	1.17	1701	6	1HP + 2LP

## 3. Engine Cycle

### A. Baseline Engine

As it is mentioned previously, the baseline engine for JULIO is the Rolls Royce/SNECMA Olympus 593 Mk 610, which was the Concorde's engine. An engine cycle model of the Olympus 593 was made using the software GasTurb13 [11] (see Figure 1) because it makes a comparison point and a reference to continue with the respective optimization. GasTurb13 software was also chosen because it was the most graphical and understandable one of those

tried: MDIDS-GT and AxSTREAM.

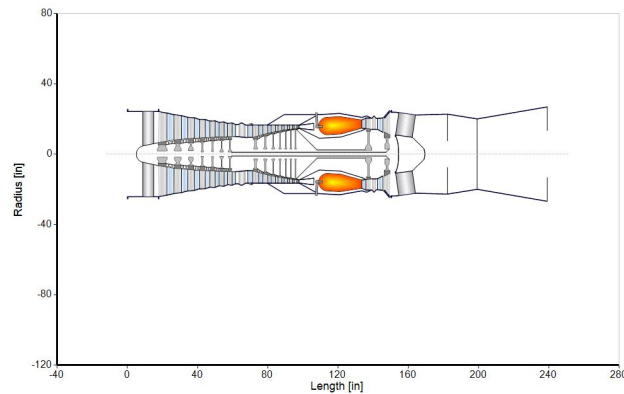


**Fig. 1 Rolls Royce/SNECMA Olympus 593 GasTurb13 engine model.**

Although the use of this software implied its empirical use and losing information about initial weights and operation maps that provide valuable data, it was used because this software provides a graphical way to see and understand the cycle. All the input data was given by the respective request for proposals of this contest. The discrepancies between the GasTurb13 model and the RFP baselines are small, the only difference is 0.01% in the thrust being this a negligible difference.

The cycle results of the Olympus 953 GasTurb13 model are shown in the Figure 2 considering a service ceiling of 53000 ft and a cruise velocity of Mach 2.

Station	W lb/s	T R	P psia	WRstd lb/s		
amb		389,97	1,456		FN	= 10031,95 lb
1	289,345	701,78	11,402		TSFC	= 1,3304 lb/(lb*h)
2	289,345	701,78	10,684	462,971	FN/W2	= 1115,51 ft/s
24	289,345	1098,53	43,803		WF Burner	= 3,70746 lb/s
25	289,345	1098,53	43,365	142,705	P2/P1	= 0,9370
3	289,345	1537,76	125,757	58,221	P25/P24	= 0,9900
31	257,517	1537,76	125,757		P3/P2	= 11,7711]
4	261,224	2430,00	120,727	68,828	P45/P44	= 0,9800
41	275,692	2385,73	120,727	71,975	P6/P5	= 0,9800
43	275,692	1965,47	47,934		W_NGV/W25	= 0,05000
44	290,159	1944,88	47,934		WHc1/W25	= 0,05000
45	290,159	1944,88	46,976	175,776	WLc1/W25	= 0,00000
49	290,159	1589,72	18,800		XM6	= 0,50000
5	290,159	1589,72	18,800	397,100	A8	= 1247,57 in²
6	290,159	1589,72	18,424		WB1d/W2	= 0,01000
8	290,159	1589,72	18,424	405,204	Ang8	= 20,00 °
Bleed	2,893	1537,76	125,757		CD8	= 0,96000
-----						
Efficiencies:	isentr	polytr	RNI	P/P		
LP Compressor	0,8530	0,8782	0,507	4,100	P8/Pamb	= 12,65199
HP Compressor	0,8170	0,8402	1,208	2,900	W1kLP/W25	= 0,00000
Burner	0,9900			0,960	Loading	= 100,00 %
HP Turbine	0,8900	0,8785	1,378	2,519	e444 th	= 0,85985
LP Turbine	0,9000	0,8890	0,677	2,499	W1k0/W25	= 0,00000
-----						
HP Spool mech Eff	0,9900	Nom Spd	8382	rpm	PWX	= 100,0 hp
LP Spool mech Eff	0,9900	Nom Spd	5819	rpm	Core Eff	= 0,5425
-----						
Con-Di Nozzle:					Prop Eff	= 0,7778
A9*(Ps9-Pamb)	1536,275				A9/A8	= 1,80000
-----						
hum [%]	war0	FHV	Fuel		CFGid	= 0,95633
0,0	0,00000	18552,4	Generic			

**Fig. 2 Rolls Royce/SNECMA Olympus 593 modeling results in GasTurb13.**

## B. Engine Type Definition

In order to establish the most appropriate engine architecture to satisfy the design requirements, three different configurations are analyzed, in which the values of net thrust, TSFC and fuel consumption (WF) are crucial to determine the best suitable engine type; the configurations analyzed are: separate flow turbofan, mixed turbofan with afterburner and without afterburner. For this, the performance of each one in cruise and takeoff is taken into account based on the parameters in Table 3, the results are presented in the Table 5.

**Table 5 Engine Comparison Parameters. From [11].**

	Takeoff			Cruise		
	FN [lbf]	TSFC [lb/(lbh)]	WF [lb/s]	FN [lbf]	TSFC [lb/(lbh)]	WF [lb/s]
<b>Separate Flow Turbofan</b>	25445.27	0.95	6.77	7689.27	1.61	3.45
<b>Mixed Turbofan</b>	33609.48	1.07	10.07	10000.19	1.30	3.63
<b>Mixed Turbofan - Reheat</b>	33612.46	1.13	10.64	14792.03	1.45	5.97

Based the data from Table 5, the turbofan configuration does not meet the thrust at either of the two operating points required for the design. The Mixed Turbofan and the Mixed Turbofan - Reheat do. After reviewing the thrust factor, the

TSFC and the WF, the Mixed Turbofan has lower consumption. This is because his average gas flow rate decreases, losses at the output speed decrease, and the engine flight efficiency increases [14]. For this reason it is decided that the JULIO configuration will be Mixed Turbofan without Reheat as it can satisfy the operating conditions and the fact of not needing afterburner represents a saving in fuel consumption and less weight for the engine.

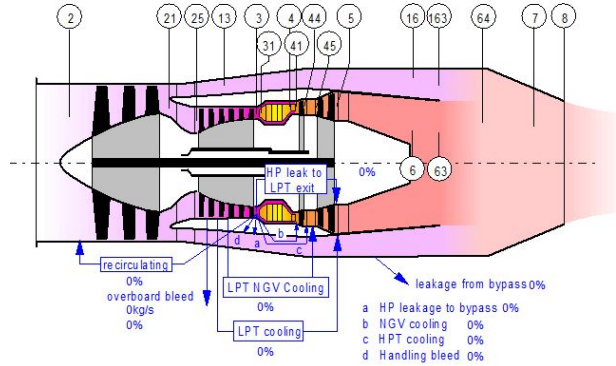


**Fig. 3 Mixed Flow Turbofan Architecture**

## 4. Inlet

### A. Description

The engine JULIO features the same characteristics in the inlet of the Olympus 593 since the inlet shares the general structure of the Concorde, supplying the correct air mass flow at the specific conditions of velocity and pressure required for the optimal engine operation.

Considering that the inlet is a structural component of the Concorde itself, some conditions were given by the RFP [8] as it is shown below at the Table 6.

**Table 6 Inlet Flight Conditions.**

	<b>Off-Design</b>	<b>On-Design</b>
Intake Pressure Recovery	0.937	0.983
Flight Condition	takeoff	Cruise

The Concorde's inlet is designed to supply air subsonic conditions to the engine, reducing the velocity of the air flow from Mach 2 in the outside to an engine inlet velocity of Mach 0.6 by a convergent-divergent geometry, it also provides a rise of the pressure ratio by 7:1. [15]

According to the characteristics of the inlet that could be investigated and in addition to the information provided by

the RFP, the use of a 2D variable inlet is still the best option as it is used in the Concorde. [16]

**Table 7 Inlet Geometry Information.**

Parameter	Value
Number of struts	8
Gap Width/Height	0.2
Cone Length/Radius	0.5
Cone Angle [deg]	35
Casing Length/Radius	0.5
Casing Thickness [in]	0.19685

In Table 7 the geometry data of the inlet.

## B. Materials and Manufacturing

Stainless steel is recognized for high corrosion resistance, good ductility, high impact toughness. Made with an iron base and elements such as chromium, manganese, silicon, nickel, aluminum, carbon, phosphorus and sulfur, we have ASTM S40500 stainless steel. This material is subjected to an annealing heat treatment in order to improve the mechanical properties of the material: as ductility and correct his internal grain structure. Due to his characteristics, it is ideal for the motor inlet.

**Table 8 Material Properties.**

Properties		Units
Density	0.282	lb/in <sup>3</sup>
Yield strength (0.2%)	39885.38	psi
Tensile strength	69618.11	psi
Maximum service temperature	1931.4	°R

## 5. Compressors

Initially the JULIO includes a 3-stage fan (or LP compressor) and a 5-stage high pressure compressor. The selection of the number of stages was made based on the models presented in the section 3, with the idea in mind of reduce the weight and engine's dimensions, but that it meets the thrust and temperature requirements, with the YJ-2030 engine being the baseline engine that best suited this criterion (3-stage fan with a 6-stage HP) [6]. Once these requirements were achieved, the team use GasTurb13[11] to do an optimization phase, where the main objective was to obtain as much as airflow as possible. Due to temperature restrictions, the decision of maintain the configuration presented above

was made.

## A. Fan - Low Pressure Compressor

### 1. Design Criteria

Following the trend presented in section 3, the fan will have 2 functions: Work as a low pressure compressor and move enough airflow to achieve the desired thrust. In that order of ideas, it was defined that the fan will have 3 stages, generating an inner fan pressure ratio of 1.233 and an outer fan pressure ratio of 1.866. The pressure ratio conditions presented above were achieved after an iterative optimization process, using GasTurb13 software. The aim was to find the lowest specific fuel consumption possible by maintaining the required thrust as constant and varying the bypass ratio, high pressure compression ratio and fan pressure ratios.

As can be seen in the fan's operation map (see Figure 4), it operates under conditions that allow it to be out of risks such as fan blade stall and subsequent surge.

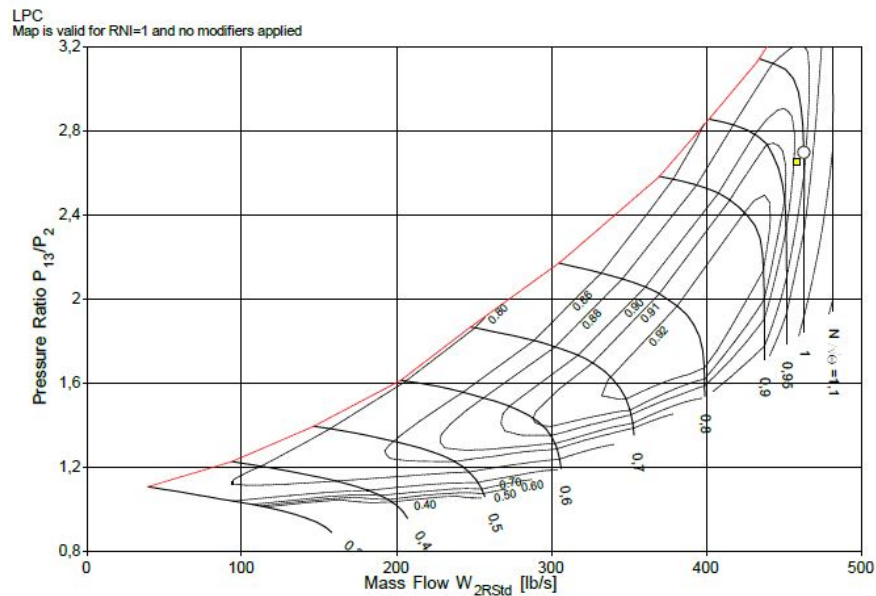


**Fig. 4 Fan Operation Map.**

### 2. Geometry

Thanks to the optimization process mentioned above, it was possible to have a bypass ratio of 0.98. Therefore, the fan diameter is 47.75 in, managing to meet the objective of not increasing the front area of the engine.

In the Figure 5 is possible to see the fan's architecture of the JULIO engine.

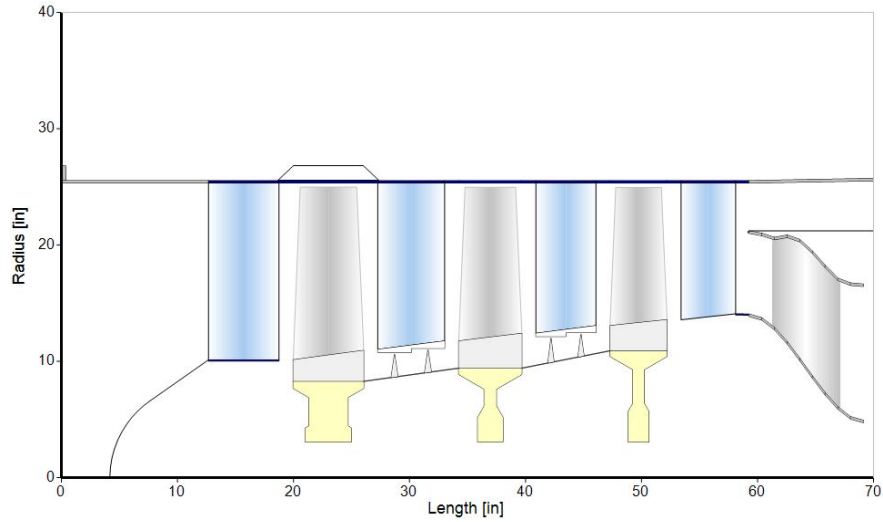


**Fig. 5 Fan architecture.**

### 3. Fan Design Results

As mentioned above, the fan is made up of 3 stages, which are driven by the shaft that is fed by the low-pressure turbine. In the Table 9 is possible to see all design parameters of the fan.

**Table 9 Fan Specifications.**

Parameter	Value	Parameter	Value
Total Temperature [ $^{\circ}$ R]	717.9	IGV Profile Thickness [%]	5
Total Pressure [psi]	10.683	Spool Speed [RPM]	7120.84
Mach Number	0.55	Inlet Tip Diameter [in]	50.68
Mass Flow [lb/s]	286.074	Inlet Hub Diameter [in]	20.27
Polytropic Efficiency [%]	90	Inner Fan Pressure Ratio	1.233
Fan Area [in <sup>2</sup> ]	1790.75	Outer Fan Pressure Ratio	1.86672
Number of Stages	3	Bypass Ratio	0.98

### B. Materials and Manufacturing

The material selected for the Fan is a thermoplastic with a semi-crystalline structure, the material prepared for a high demand is reinforced with 30% carbon fiber in order to reduce its density and improve its mechanical resistance. Due to the operating conditions of the material “PEEK (30% Carbon Fiber)” it is ideal for the operation of the fan. The properties are specified in the Table 10

**Table 10 Material Properties.**

Properties	Units	
Density	0.052	lb/in <sup>3</sup>
Yield strength (0.2%)	33068.6	psi
Tensile strength	33068.6	psi
Maximum service temperature	995.67	°R

### C. High Pressure Compressor

For JULIO this is composed of 5 stages, which gives a pressure ratio of 8.89. It was also required to comply with certain characteristics that restricted the design of a compressor with performance at high temperatures. To meet these requirements, a HPC was designed that meets both take-off and cruise conditions, in all cases it was necessary to analyze in detail the mass flows established in the RFP and the temperatures that it reaches. The design of the HPC was established under on-design conditions, then with the aim of complying with the necessary thrust, the respective optimization was carried out in off-design. The Table 11 summarizes the operation conditions of the high-pressure compressor.

**Table 11 High-Pressure Compressor Operating Conditions.**

Parameter	Value
Static Temperature [°R]	1485.53
Static Pressure [psi]	115.949
Mass Flow [lbm/s]	144.454
Pressure Ratio	8.89
Polytropic Efficiency [%]	90

#### 1. Design Criteria

As it was mentioned above (in section 5), the design parameters for the HP compressor were obtained by a iterative optimization process (using GasTurb13 [11]) where the objective was to reduce the specific fuel consumption changing the compressor pressure ratio, the bypass ratio and the fan pressure ratio, but keeping enough thrust to accomplish with both on-design and on-design conditions requirements. Some of the initial parameters chosen following authors like Saravanamuttoo [17], Mattingly [1] and Farokhi [18]. The Table 12 shows the design results of the high-pressure compressor.

The Figure 6 shows the high-pressure compressor operation map, which shows that the compressor operates under

**Table 12 High-Pressure Compressor design results.**

Parameter	Value	Parameter	Value
Number of Stages	5	Spool Speed [RPM]	10097.96
Number of IGV	1	Inlet Tip Diameter [in]	32.9
Tip Speed [ft/s]	1450	Inlet Hub Diameter [in]	9.87
Inlet Mach Number	0.55	Pressure Ratio	8.89

the permissible limits, far from the the stall lines.

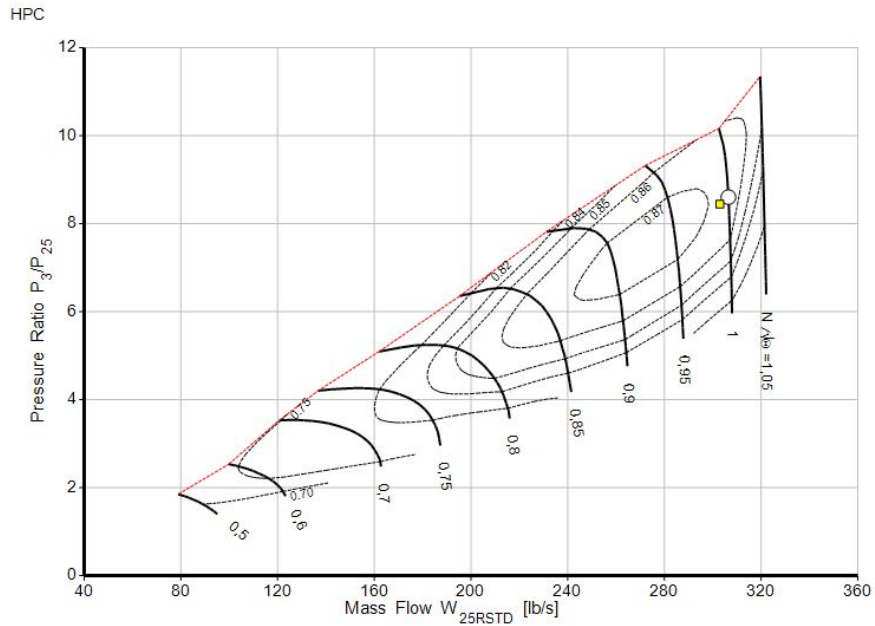


**Fig. 6 High-Pressure Compressor operation map.**

## 2. Geometry

The high-pressure compressor consists of 5 stages plus an inlet guide vanes (IDV), generating a pressure ratio of 8.89, fulfilling the objective of having the fewest possible stages.

In Figure 7 it is possible to see the architecture of the high-pressure compressor of the JULIO engine.

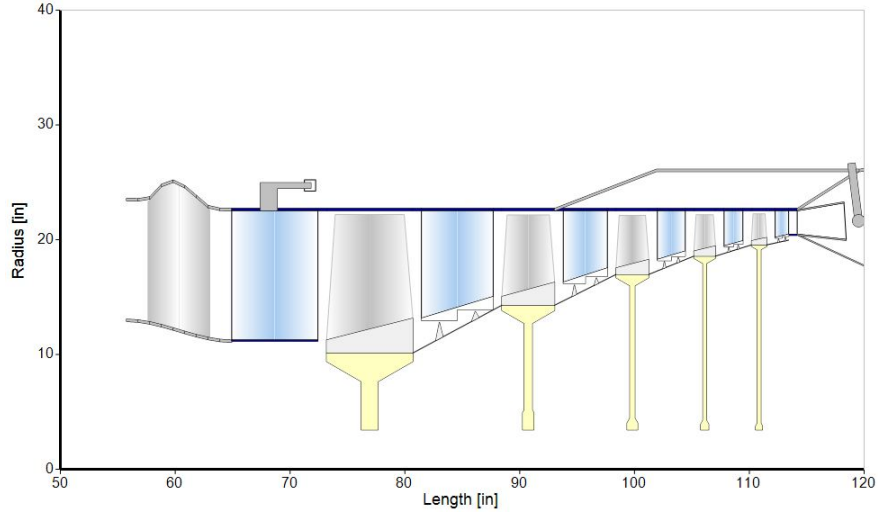


**Fig. 7 High-Pressure Compressor architecture.**

#### **D. Materials and Manufacturing**

Due to the compressor operating conditions, the most optimal material is a super nickel alloy due to the properties they present. “UDIMET 700” withstands demanding engine conditions such as high temperatures, creep resistance and corrosion resistance. The material has the following characteristics.

**Table 13 Material Properties.**

<b>Properties</b>	<b>Units</b>	
<b>Density</b>	0.285	lb/in <sup>3</sup>
<b>Yield strength (0.2%)</b>	155190.4	psi
<b>Tensile strength</b>	226258.9	psi
<b>Maximum service temperature</b>	2507.4	°R

### **6. AVC-8015 Combustion Chamber**

#### **A. Design Point**

The design point chosen for the combustion chamber is the supersonic cruise cycle where the inlet temperature in the turbine (3150 °R) is the highest in the AVC-8015 combustor [8]. Table 14 shows the inlet conditions for the combustion chamber at the design point. Those values are taken from the compressor cycle analysis.

**Table 14 Combustor Inlet Condition.**

Parameter	Symbols	Value	Units
Total Temperature at Inlet	$T_{t,3}$	1485.53	°R
Static Temperature at Inlet	$T_{s,3}$	1475.22	°R
Total Pressure at Inlet	$P_{t,3}$	115.94	Psi
Static Pressure at Inlet	$P_{s,3}$	112.86	Psi
Velocity at Inlet	$V_3$	370.02	ft/s
Mach Number at Inlet	$M_3$	0.2	-
Air Mass Flow Rate at Inlet	$\dot{m}_3$	144.45	lb/s
Air Mass Flow Rate at Outlet	$\dot{m}_4$	130.64	lb/s
Air Density at Inlet	$\rho_3$	0.20	lb/ft <sup>3</sup>
Fuel-to-Air Ratio at Outlet	$far_4$	0.02	-

**B. Type of the combustion**

According to Yize Liu [19] in a Lean Direct Injection (LDI) combustor, vaporized fuel is injected directly to the combustion chamber — as minimizes the risk of flashback and auto-ignition — and is rapidly mixed with a large concentration of air. It helps to maintain an overall mixture equivalence ratio fuel lean, as stated by Xiao Ren [20]. The highest temperature at medium to high power can be reduced if the fuel and air are properly mixed before the reaction is completed. The LDI injector occupies a big portion of the dome area to allow the large fraction of the total air, from 60-70 percent of the air goes through the injector system and the remaining is for cooling. [19].

The configuration of a LDI combustion chamber demand a short length, meaning less weight for the engine. Also, addresses the issue of high  $NO_x$  emissions, as this technology is known for their low  $NO_x$  emissions (by minimizing flame temperature, according to [21]) and low smoke, meeting the design objectives of the RFP [8].

**C. Combustor Design***1. Type of Combustor*

An annular combustion chamber was chosen based on the advantages that it has compared to the other kind of combustion chambers, as the length of the chamber is 75 percent of that of a can-annular system and the wall area is much less, approximately 15 percent (of the same diameter). These characteristics result in a reduction in the amount of cooling air needed and the problem of combustion propagation from chamber to chamber is eliminated [22].

## 2. Diffuser Design

For AVC-8015 one of the most important design objectives is to reduce the weight compared to the Olympus 593 combustor [8]. According to these conditions and taking into account the Figure 8, the Dump diffuser is chosen for the AVC-8015 combustor. This because the saving in weight and stability for several flight conditions make it the ideal candidate for the diffuser design. However, due to the flow separation generated by the dump diffuser, sufficient axial length is needed for the separated flow to eventually rejoin the downstream diffuser walls, causing large pressure losses to limit design and performance parameters for this type of diffusers [1].

According to Mattingly [1], the best possible flat-wall diffuser has an included angle of  $2\theta = 9$  deg, a corresponding area ratio AR in the range of  $1.5 < AR < 4$  and a maximum diffusion efficiency  $n_{D9}$  of 0.91 by Eq. (9.68) of Ref. [1]. If the required area ratio AR is less than four, the excessive diffuser length can be reduced by subdividing the flow into adjacent streams, each with an included angle of  $2\theta = 9$  degrees. For this reason, to improve pressure losses, the AVC-8015 diffuser geometry incorporates two equally spaced splitter plates to obtain a dividing factor equal to the number of parallel streams that allow an  $AR < 4$  as shown in Figure 9. In addition, an exhaust pipe of length  $L_d = (H_2 - H_m)$  is required to separate flow at the discharge diffuser inlet has a sufficient axial distance to rejoin the upper and lower wall [1].

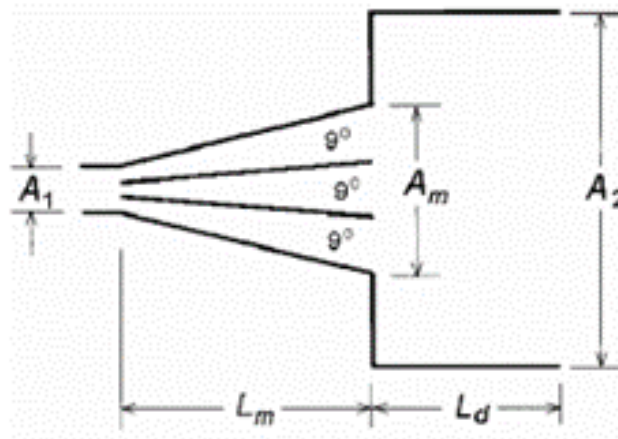


**Fig. 9 Combined Diffuser Geometry. From [1]**

The total pressure loss of the annular dump diffuser with two splitters plates is obtained by Eq.6.1 with the assumption of uniform, steady, incompressible flow with negligible friction.[1]

Diffuser Type	Merits	Drawbacks
Aerodynamic or faired	Low pressure loss	Relatively long Performance susceptible to thermal distortion and manufacturing tolerances Performance and stability sensitive to variations in inlet velocity profile
Dump	Relatively short Insensitive to variations in inlet flow conditions	Pressure loss about 50% higher than for faired type
Vortex-controlled	High performance Short length Low pressure loss	Requires minimum of 4% air bleed Design procedures not fully established
Hybrid	High performance Short length Low pressure loss Low bleed air requirement	Design procedures not fully established Bleed air pressure too low for turbine cooling
Hybrid with prediffuser	High performance Low pressure loss Low bleed air requirement High bleed air pressure	Needs extra length

**Fig. 8 Relative Merits of Various Diffuser Types. From [2]**

$$\Delta P_t = q_1 \left( 1 - \frac{1}{AR^2} \right) (1 - n_D) \quad (6.1)$$

Where AR is the area ratio which equals  $A_2/A_1$ ,  $q_1$  is the inlet dynamic pressure of combustor and  $n_D$  who can be calculated in the Eq. 6.2, is the efficiency of the whole diffuser combined by the flat-wall and dump diffuser. [1]

$$n_D = \frac{n_{D9} AR^2 \left[ \frac{A_1}{A_m} \right]^2 + 2 \left( AR \left[ \frac{A_1}{A_m} \right]^2 - 1 \right)}{AR^2 - 1} \quad (6.2)$$

The dump diffuser geometry parameters and calculated results are listed in Table 15.

### 3. Combustor Geometry

**Combustor Length:** According to Mattingly [1] in chapter 10.6.4, the length of main burners varies with the pressure and temperature and is unaffected by the size of the engine. The relation is as follows:

$$L \alpha \frac{P_{t,3}^{-r}}{\sqrt{T_{t,4}}} \quad (6.3)$$

**Table 15 Diffuser calculation.**

Parameter	Symbols	Value	Units
Inlet Area of Diffuser	$A_1$	191.41	In <sup>2</sup>
Outlet Area of Flat-Wall	$A_m$	349.95	In <sup>2</sup>
Outlet Area of Dump Region	$A_2$	681.72	In <sup>2</sup>
Mach number at Diffuser inlet	$M_3$	0.2	-
Mach number at Diffuser outlet	$M_{31}$	0.06	-
Total Pressure at Difusser Region Inlet	$P_{t,3}$	115.95	Psi
Total Pressure at Difusser Region Exit	$P_{t,31}$	115.38	Psi
Pressure Loss in the Diffuser	$dP$	0.56	Psi
Pressure Loss percentage in the Diffuser	-	0.48	%
Diffuser Length ( $L_m + L_d$ )	$L$	5.11	In
Diffuser Area Ratio	$AR$	3.58	-
Diffuser Efficiency	$n_D$	80	%

Where  $P_{t,3}$  is the total pressure at the entrance of the combustor,  $T_{t,4}$  is the total temperature of the turbine, and  $r$  could get two values: 1.51 under normal pressure conditions or 0.714 for operations at really high pressure (maximum power) [1]. This relation explains the trend of shortening the main burner length with increases in compressor pressure ratio. To make the relationship, the following combustion chambers can be considered. See Figure 10.

Engine type	TF39 Annular	TF41 Cannular	J79 Cannular	JT9D Annular	F100 Annular	T63 Can
Mass flow						
Air, lb/s	178	135	162	242	135	3.3
Fuel, lb/h	12,850	9965	8350	16,100	10,580	235
Size						
Length, in.	20.7	16.6	19.0	17.3	18.5	9.5
Diameter, in.	33.3	5.3/24.1 <sup>a</sup>	6.5/32.0 <sup>a</sup>	38.0	25.0	5.4
$P_{t3}$ , psia	382	314	198	316	366	92
$T_{t4}$ max, °R	2915	2620	2160	2865	3025	1840

**Fig. 10 Combustor Data to obtain the length ratio in Eq. 6.3. From [1]**

For AVC-8015, the operation conditions described in Table 14 for on-design gives  $P_{t,3}$  a value of 115.949 *Psi* and  $T_{t,4}$  from the RFP [8] is 3150 °R. Now from the most critical condition:

$$\frac{P_{t,3}^{-r}}{\sqrt{T_{t,4}}} = 0.000598 \quad (6.4)$$

From Figure 10, the combustion chamber most similar to operating conditions is the JT9D annular chamber engine at a 75 percent ratio. Finally, considering the result of the Eq. 6.4, the length of the AVC-8015 combustion chamber is

presented in Table 16.

**Combustor Diameter:** From Eq. 6.5, it is possible to find the area of the combustion chamber considering the analysis of the cycle the parameters of mass flow and density at the entrance of the combustion chamber. For Velocity, the output value of the dump diffuser raised in Table 15 is taken. [2].

$$\dot{m} = \rho VA \quad (6.5)$$

From the area, the radial height  $H_r$  value or diameter of the combustion chamber can be found considering the external radius and the internal radius, these data are taken from the analysis in the engine cycle [2]. The parameters and calculated results are found in Table 16.

**Table 16 Combustor geometry calculation.**

Parameter	Symbols	Value	Units
Combustor Radial Height	$H_r$	8.01	In
Combustor Length	$L_c$	33.75	In
Combustor Area	$A_c$	964.04	In <sup>2</sup>

#### 4. Burner Pressure Loss

According to Mattingly [1] in chapter 10.6.5, an estimate of the total pressure loss resulting from increasing the gas total temperature and frictional loss of a combustion system can be obtained by modeling the combustion system as a constant-area duct with simple heating (increase in total temperature) and internal drag proportional to the incoming dynamic pressure. The gas is assumed to be calorically perfect at inlet  $i$  and exit  $e$ , and the mass addition of fuel is neglected in comparison to the air mass flow. Therefore, taking into account the basic equations of fluid dynamics for mass and momentum, equations 6.6 and 6.7 are presented as a solution to the estimation of the total pressure loss [1].

$$M_e^2 = \frac{2\phi}{1 - 2\gamma_e\phi + \sqrt{1 - 2(\gamma_e + 1)\phi}} \quad (6.6)$$

$$\frac{P_{te}}{P_{ti}} = \frac{P_e}{P_i} \frac{\{1 + [(\gamma_e - 1)/2] M_e^2\}^{\gamma_e/(\gamma_e - 1)}}{\{1 + [(\gamma_i - 1)/2] M_i^2\}^{\gamma_i/(\gamma_i - 1)}} \quad (6.7)$$

Where  $\frac{P_e}{P_i}$  and  $\phi$  are:

$$\frac{P_e}{P_i} = \frac{1 + \gamma_i M_i^2 \left(1 - \frac{C_D}{2}\right)}{1 + \gamma_e M_e^2} \quad (6.8)$$

$$\phi = \frac{\gamma_i M_i^2 \left\{1 + [(\gamma_e - 1) / 2] M_e^2\right\} T_{te}}{\gamma_e \left[1 + \gamma_i M_i^2 \left(1 - \frac{C_D}{2}\right)\right]^2 T_{ti}} \quad (6.9)$$

For convenience, the equation for total temperature ratio can be written in terms of engine temperature ratios as [1].

$$\frac{T_{te}}{T_{ti}} = \frac{T_{t4}}{T_{t3}} \quad (6.10)$$

Considering the following parameters in Table 17 and equations above for AVC-8015, the Figure 11 corresponding to the graphic of the total pressure loss in the AVC-8015 combustion chamber. Also, Table 17 presents the results obtained from the graph of Figure 11.

**Table 17 Combustor Pressure Parameters.**

Parameter	Symbols	Value	Units
Combustor Total Temperature at Inlet	$T_{t,3}$	1485.53	°R
Combustor Total Temperature at Outlet	$L_{t,4}$	3150	°R
Drag Coefficient	$C_D$	0.5	-
Air Heat Capacity Ratio	$\gamma_i$	1.4	-
Gas Heat Capacity Ratio	$\gamma_e$	1.33	-
Combustor Mach Inlet	$M_i$	0.06	-
Pressure Drop	$\frac{P_{te}}{P_{ti}}$	0.971	-
Combustor Pressure Loss		2.9	%

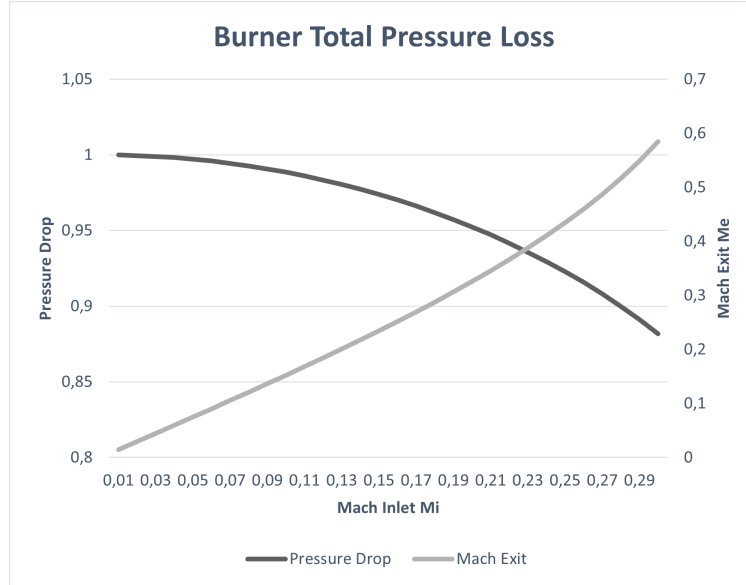


**Fig. 11 Combustor Total Pressure Loss.**

The results of the Figure 11 from the Table 17 show that the combustion chamber with a Mach inlet  $M_i$  of 0.06 presents a reasonable total pressure ratio ( $P_{te}/P_{ti} = 0.971$ ) resulting from the increase of the gas total temperature and the friction in the combustor. According to Mattingly [1], this loss ratio equivalent to 2.9 % for AVC-8015 combustor is within the loss ranges ( $2 < \% < 8$ ) for the adverse pressure gradient generated by aerodynamic phenomena (vortex) in the primary zone of the combustion chamber it doesn't cause instability in the cycle and a great loss of static pressure.

### 5. Burner Efficiency

Because propulsion system fuel consumption has a direct effect on aircraft system range, payload, and operating cost, design-point combustion efficiency must be as close to 100 percent as possible [1]. For conditions off design, the efficiency must be in the order of 98.5 percent to satisfy regulations on exhaust carbon monoxide and unburned hydrocarbons [1]. One analytical method to test if the efficiency is in this range is based on the reaction rate parameter and is plotted in the Figure 12.

Analytically is defined as:

$$\theta = \frac{P_{t3}^{1.75} A_{ref} H \exp\left(\frac{T_{t3}}{b}\right)}{\dot{m}_3} \times 10^{-5} \quad (6.11)$$

Where  $P_{t3}$  is the main burner pressure in [psi],  $A_{ref}$  is the main burner reference area [ $in^2$ ], H is the height of the

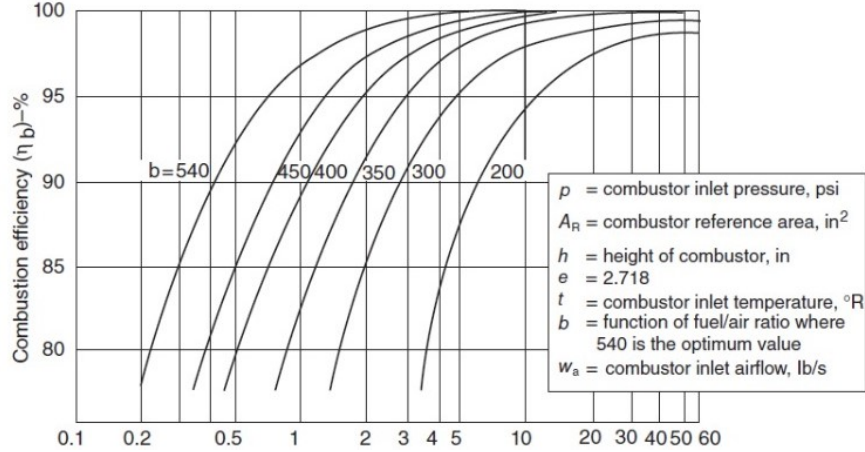


**Fig. 12 Combustion efficiency correlation. From [3]**

main burner [in],  $T_{t3}$  is the main burner temperature inlet [R],  $m_3$  is the main burner inlet airflow [lbm/s] and  $b$  is the function of local equivalence ratio, the last one is defined by the Eq. 6.12. [1].

$$b = 385(\sqrt{2} \pm \ln(\frac{\phi}{1.03})) \quad (6.12)$$

where plus is used when  $\phi < 1.03$  and minus when  $\phi > 1.03$ . [1].

As stated by Xiao Ren [20],  $\phi$  has the value of 0.55 for an LDI combustor, and for that, the value of  $b$  is equal to 302.92.

The rest of the parameters and the value of  $\theta$  are listed in the Table 18.

**Table 18 Reaction Rate Parameters.**

$b$	$P_{t3}$ psi	$A_{ref}$ $in^2$	H in	$T_{t3}$ $^{\circ}R$	$\dot{m}_3$ lbm/s	$\theta$
302.92	115.95	964.04	8.02	1485.53	144.45	295.55

Following the graph of Combustion efficiency vs reaction rate parameter in the Figure 12, it is concluded that the efficiency of the combustion is 99.1 percent.

## D. Fuel System

### 1. Fuel Injection

AVC-8015 will feature fuel atomizers with an airspray nozzle system. This is because by aerating the spray, local concentrations rich in fuels can be avoided, which reduces carbon formation and exhaust smoke. In addition, from this

process lower pressures required for atomization of the fuel can be obtained. [22].

## 2. Number of Fuel Injectors and Fuel atomizing Flow

According to Mattingly [1], an airspray atomizer typically requires about 3 Lbm of primary air per Lbm of fuel. For a single array, the number of fuel nozzles required can be calculated by dividing the annular flow passage into square segments as follow. [1].

$$N_{noz} \approx \frac{\Pi (r_o + r_i)_{3,2}}{H_r} = \frac{A_{3,2}}{H_r^2} \quad (6.13)$$

Where  $H_r$  is radial height and  $A_{3,2}$  is assumed the area of the combustion chamber calculated in the Table 16 . The  $N_{noz}$  parameter and fuel atomizing flow  $W_{am}$  calculation are listed in Table 19.

**Table 19 Number of Fuel Injectors and Fuel Flow parameters calculation.**

Parameter	Symbols	Value	Units
No. of Fuel Injectors	$N_{noz}$	13	-
Fuel Flow	$W_f$	3.63	Lb/s
Atomize Air to Fuel Ratio	$AFR$	3	-
Atomizing Flow Calculation Flow	$W_{am}$	10.90	Lb/s

## E. Materials and Manufacturing

AVC-8015 is composed of a Nimonic 263<sup>tm</sup> nickel–chromium–cobalt–molybdenum alloy specially designed for use in high temperature and high resistance applications, especially for hot section components of gas turbines or combustion chambers. The required physical properties of Nimonic Alloy 263<sup>tm</sup> are described in Table 20. [12].

**Table 20 Required physical properties of Nimonic Alloy 263<sup>tm</sup>. From [12].**

Properties	Metric	Unit	Imperial	Unit
Density	8.36	$g/cm^3$	0.302	$lb/in^3$
Melting Point	1300-1355	°C	2831.67-2930.67	°R

## F. Cooling or Refrigeration

This section identifies and briefly describes the airflow distribution terminology in, around, and through the main burner, resulting in the four basic airflow regions illustrated in Figure 13.

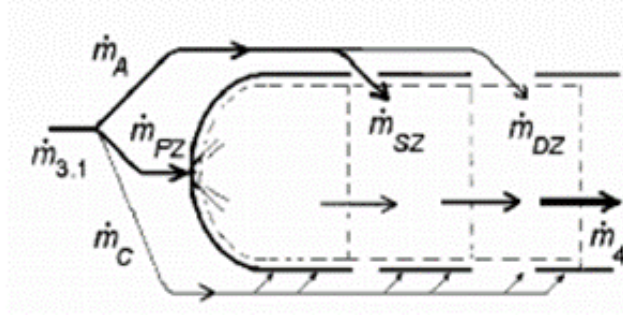


Fig. 13 Schematic and nomenclature for air partitioning. From [1].

Cooling air must be used to protect the burner liner and dome from the high radiative and convective heat loads produced within the burner. This air is normally introduced through the liner such that a protective blanket or film of air is formed between the combustion gases and the liner hardware. [1].

**The primary zone:** According to Mattingly [1] in the chapter 9.2.2.1, the primary zone equivalence ratio can be solved using the Eq. 6.14. Where  $\varepsilon_{pz} = 0.7$  from [1] design target.

$$\phi_{pz} = \frac{T_g - T_{t,3.1}}{\varepsilon_{pz} \Delta T_{max}} \quad (6.14)$$

And the corresponding primary zone air flow rate  $\dot{m}_{pz}$  and flow fraction  $\mu_{pz}$  are in the Eq. 6.15 and Eq. 6.16. Where  $f_{st}$  for representative jet fuel is  $0.0685 \text{ lbmF/LbmA}$ . from [1].

$$\dot{m}_{pz} = \frac{\dot{m}_f MB}{f_{st} \phi_{pz}} \quad (6.15)$$

$$\mu_{pz} = \frac{\dot{m}_{pz}}{\dot{m}_{3.1}} \quad (6.16)$$

Primary zone parameters and calculated results are listed in Table 21.

**Liner Cooling:** The effectiveness of the cooling technique is quantified by the cooling effectiveness  $\Phi$ , defined by Eq. 6.17.

$$\Phi = \frac{T_g - T_m}{T_g - T_c} \quad (6.17)$$

where  $T_g$ ,  $T_m$  are the static temperatures of the mainstream gas, average wall material limit, and cooling air, respectively. Note that  $T_c = T_{t,31}$  is the total temperature at the outlet of the diffuser. While the wall material was chosen as Nimonic Alloy 263<sub>tm</sub> mentioned above,  $T_m$  equals 2370 °F or 2829.67 °R from Table 20. Figure 14 presents the cooling air mass flow rates for varying values of cooling effectiveness. [1].

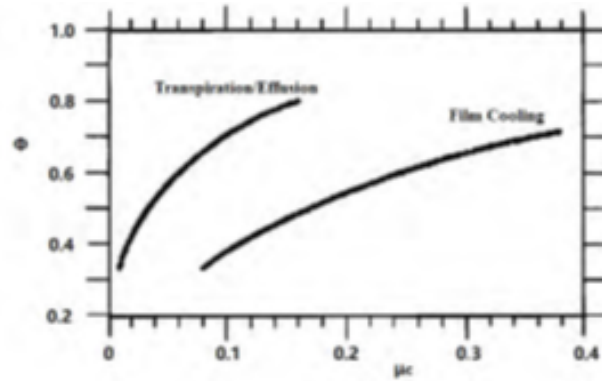


**Fig. 14 Air Flow  $\mu_c$  fraction required for given cooling effectiveness  $\Phi$ . From [1].**

Equation 6.18 are approximate curve fits Figure 14 and provide approximate design data for the fraction of main burner airflow required to achieve any desired cooling effectiveness. [1].

$$\mu_c \doteq \frac{\dot{m}_c}{\dot{m}_{3,1}} \cong \frac{\Phi}{6(1 - \Phi)} \quad (6.18)$$

Liner cooling parameters and calculated results are listed in Table 21.

**Secondary zone and Dilution Zone:** According to Mattingly [1] in the chapter 9.2.2.3, the equivalence ratio at secondary zone exit  $\phi_{sz}$  is determined to be by Eq. 6.19.

$$\phi_{sz} = \frac{\dot{m}_{fMB}}{f_{st}(\dot{m}_{pz} + \dot{m}_{sz})} \quad (6.19)$$

from which the secondary zone mass flow fraction is determined to be by Eq. 6.20.

$$\mu_{sz} \doteq \frac{\dot{m}_{sz}}{\dot{m}_{3.1}} = \frac{\dot{m}_f MB}{\phi_{sz} f_{st} \dot{m}_{3.1}} - \frac{\dot{m}_{pz}}{\dot{m}_{3.1}} \quad (6.20)$$

According to Mattingly [1] in chapter 9.2.2.4, the dilution zone flow factor and air mass flow are realized taking into account the Eq. 6.21.

$$\mu_{sz} \doteq \frac{\dot{m}_{DZ}}{\dot{m}_{3.1}} = 1 - (\mu_{pz} + \mu_{sz} + \mu_c) \quad (6.21)$$

Secondary and Dilution zone parameters results are listed in Table 21.

**Table 21 Combustor Air Flow Calculation.**

Parameter	Symbols	Value	Units
Inlet Air Flow	$\dot{m}_{31}$	144.45	Lb/s
Primary Air Flow	$\dot{m}_{pz}$	75.1	Lb/s
Primary Air Flow Percentage	-	51.99	%
Liner Cooling Flow	$\dot{m}_c$	5.66	Lb/s
Liner Cooling Flow Percentage	-	3.93	%
Secondary Air Flow	$\dot{m}_{sz}$	43.06	Lb/s
Secondary Air Flow Percentage	-	29.81	%
Dilution Air Flow	$\dot{m}_{DZ}$	20.63	lb/s
Dilution Air Flow Percentage	-	14.28	%

## G. Ignition

The two igniter plug of AVC-8015 will be of the shunted surface discharge type. This is because the semiconductor chip located at the end of the insulator allows an electrical leakage of the high electrode voltage to the body that will ionize the surface of the pellet to obtain a low resistance path for the energy stored in the capacitor. Finally, this feature will allow a potential difference from the electrode to the body of only about 2000 Volts to be required for operation. [22].

## H. Emissions

The idea with the new combustor design is not only for it to be lighter and more efficient but also to attend the environmental requirements at the time the engine was introduced and in the years to come.

$CO$  and  $CO_x$  emissions harmful to the ozone layer are unavoidable in a fossil fuel burning process. However, the

way to reduce them is by looking for the highest efficiency for the different flight stages as explained later.

Today  $NO_x$  emissions play a more important role in combustion chamber design considerations.  $NO_x$  is known to poison mucous of respiratory organs, result in acid rain, delete ozone and form ozone hole. That is why for AVC-8015 the  $NO_x$  emissions index is calculated.

As reported by Wang Yingjun [23], the following equations (6.22 and 6.23) are used for a LDI combustor.

$$EI_{NO_x} = 1.539 \exp\left(\frac{T_{t,in}}{194}\right) * (far_{out})^{1.69} * \left(\frac{P_{t,in}}{1000}\right)^{-0.595} * \left(\frac{\Delta P_t}{P_{t,in}}\right)^{-0.565} \quad (6.22)$$

Where  $EI_{NO_x}$  is the emission index of  $NO_x$ ,  $P_{t,in}$  is the inlet total pressure of the combustor,  $T_{t,in}$  is the inlet total temperature,  $far_{out}$  is the outlet fuel-to-air ratio of the combustor and  $\Delta P_t/P_{t,in}$  is the total pressure loss coefficient of the combustor.

After estimating the  $EI_{NO_x}$  the LTO (landing takeoff) cycle and cruise by previous equations, the  $NO_x$  emission of LTO cycle could be calculated using following equation:

$$Emission\ Mass\ per\ unit\ of\ thrust\ \left[\frac{g}{kN}\right] = \sum \left( EI_{NO_x} \left[\frac{g}{kg_{fuel}}\right] * TSFC \left[\frac{kg_{fuel}}{KN\ hr}\right] * Time\ in\ Mode [hr] \right) \quad (6.23)$$

The following Tables (22 and 23) show the results of the emission index of  $NO_x$  and emission mass per unit of thrust for AVC-8015.

**Table 22 Emission Index of  $NO_x$ .**

$EI_{NO_x} [g/kg_{fuel}]$	
Cruise	takeoff
0.24	0.12

**Table 23 Emission Mass per unit of Thrust**

Emission Mass per unit of Thrust	
g/kN	lb/lbf
1.04	1.02E <sup>-5</sup>

Following the ICAO CAEP  $NO_x$  limits shown in the next Figure, these emissions are considered low, and they pass the regulation.

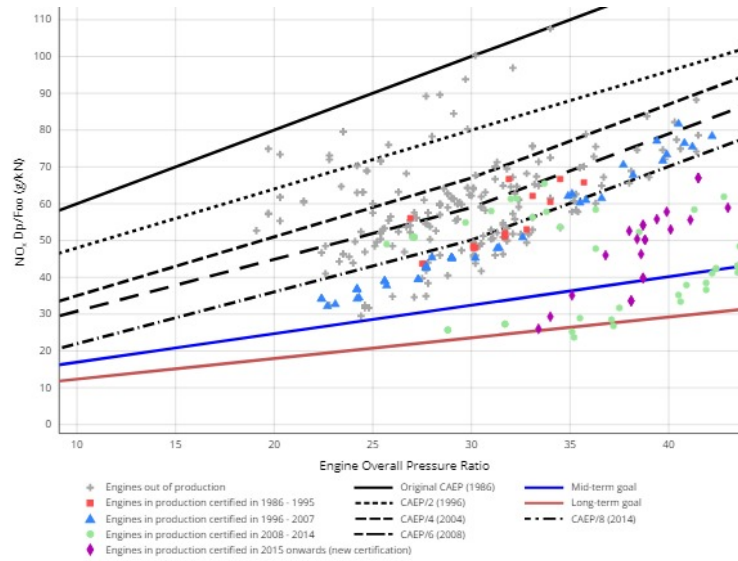


**Fig. 15 ICAO CAEP  $NO_x$  limits. From [4]**

## 7. Turbine

The turbine converts the gases kinetic energy into mechanical energy to operate the LPC, HPC and provides the power take-off for other engine-dependent systems. The JULIO turbine consists in a single HPT stage cooled by the last stage of the HPC air and a single uncooled LPT stage.

### A. High Pressure Turbine

#### 1. Design Criteria

The parameters and range of values that the authors in references [1] [18] set for the design of the HPT are taken into account. The values are summarised in the Table 24 and will be used as a reference point for the turbine stage performance conditions.

**Table 24 HPT Parameters Design Reference**

<b>Exit Nozzle Mach Number</b>	$M < 0.9$
<b>Exit Flow Angle</b>	$-40^\circ < \alpha < 70^\circ$
<b>Exit Rotor Mach Number</b>	$M < 0.9$
<b>Flow Coefficient</b>	$0.5 < \phi < 1.1$
<b>Loading Coefficient</b>	$0.8 < \psi < 2.3$
<b>Degree of reaction</b>	$0.2 < R < 0.7$
<b>Maximum <math>AN^2</math> (RPM<sup>2</sup>in<sup>2</sup>)</b>	$AN^2 < 6.5E^{10}$
<b>Loss Factor</b>	0.3 – 0.4
<b>Nozzle Axial Aspect Ratio</b>	$1 < AR < 2$
<b>Rotor Axial Aspect Ratio</b>	$1.5 < AR < 3$

2. *Smith Chart and Stages Number*

Smith’s Chart is a tool with which the efficiency of the turbine can be established by relating the Stage Flow Factor  $\phi$  defined as the ratio between the axial speed and the rotational speed and the Stage Loading Coefficient  $\psi$  depending on the enthalpy drop that occurs due to the decrease in temperature and to the energy extraction that the turbine must carry out. In this case, when performing the analysis of the cycle in GasTurb, an isentropic efficiency value of 90% is obtained for the HPT. The Smith Chart for this stage is shown below

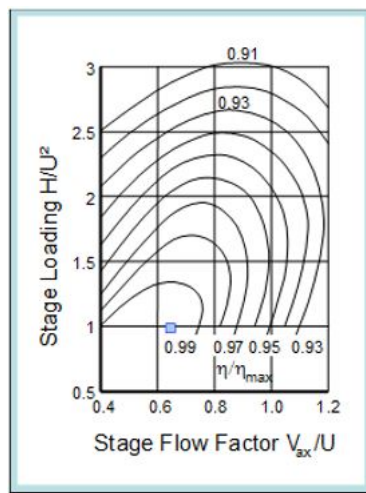


**Fig. 16 HPT Smith Chart**

According to the Figure 16, for an efficiency of 90%, the Stage Flow Factor is 0.64 and the Stage Loading Coefficient is 0.99. Considering the workload of the HPT, it was decided to place only one stage, because it extracts enough energy for the compressor to meet the operating requirements. A comparison is also made of the values indicated in Table 24,

showing that they are within the range established by the authors.

### 3. Stage Characteristics

Knowing that the isentropic efficiency of the turbine is 0.9, we proceed to find the other parameters of the stage through GasTurb13, so that the stator and rotor conditions result in the required efficiency. The initial data used to perform the procedure is organized in Table 25.

**Table 25 HPT Input Stage Data**

Property	Value	Unit
<b>HPT Rotor Inlet Dia.</b>	24.72	in
<b>HPT Rotor Exit Dia.</b>	49.99	in
<b>HPT Exit Radius Ratio</b>	0.89	-
<b>HPT Vax.exit/Vax.average</b>	1.05	-
<b>HPT Loss Factor</b>	0.35	-
<b>Interduct Mach Reference</b>	0.5	M
<b>HPT inlet temperature</b>	3150	°R

For the data indicated above, the following values in Table 26 are obtained from GasTurb13, which defines the final stage parameters.

**Table 26 HPT Output Stage Data**

Property	Value	Unit
<b>HPT Inlet radius ratio</b>	0.96	in
<b>HPT Stator Exit Angle</b>	58.25	deg
<b>HPT Exit Mach Number</b>	0.6	M
<b>HPT Exit Angle</b>	0.21	deg
<b>HPT Loss Factor</b>	0.35	
<b>HPT Rotor inlet temperature</b>	3070	°R
<b>AN<sup>2</sup></b>	4.36E <sup>10</sup>	RPM <sup>2</sup> in <sup>2</sup>
<b>Design Speed</b>	10098	RPM
<b>Number of Blades</b>	92	-
<b>Number of Vanes</b>	88	-
<b>Nozzle Axial Aspect Ratio</b>	1	-
<b>Rotor Axial Aspect Ratio</b>	1.5	-
<b>Pitch/Chord Ratio</b>	0.5	-
<b>HPT exit temperature</b>	2393.02	°R

#### 4. Velocity Diagram

After knowing the number of stages and their characteristics, the velocity diagram is plotted, the first triangle corresponds to the stator inlet and the second triangle to the rotor outlet. The Table 27 specifies the velocity values

**Table 27 HPT Velocity Values**

Property	Value	Unit
<b>Inlet V</b>	2584.06	ft/s
<b>Inlet Vax</b>	1359.41	ft/s
<b>Inlet W</b>	1359.42	ft/s
<b>Circumferential U</b>	2202.97	ft/s
<b>Exit V</b>	1427.39	ft/s
<b>Exit Vax</b>	1427.38	ft/s
<b>Exit W</b>	2620.46	ft/s
<b>Stage Loading</b>	0.99	-
<b>Stage Flow Factor</b>	0.64	-

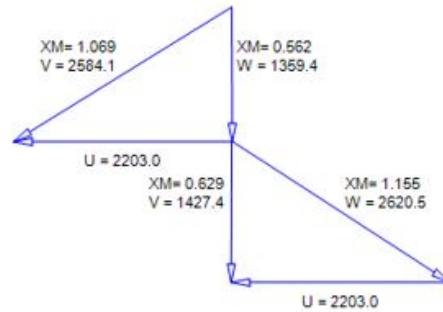


**Fig. 17 HPT Velocity Diagram**

#### 5. Turbine Blades Cooling

Since the turbine blades will be operation at very high temperature and under thermal stress due to rotation, the lifetime of the material is directly affected. Therefore it is necessary to cool the blades in order to reduce the blade temperature to an acceptable level for its correct operation [24]. Saravanamutto [17] defines film cooling as the process of extracting air from the compressor, conveying it to the turbine and discharging it through holes on the outside of the blades, generating a thin layer of air with lower temperature. One of the ways that NASA Glenn Research Center has developed to improve film cooling in the blades is to mold the shape of the holes to mitigate the separation of the flow through the cooling channels, reducing aerodynamic losses and increasing cooling efficiency, and it is also considered an easy method of manufacture and implementation [25]. Therefore, it is decided that the best option is film cooling for the HPT with the improvement proposed by NASA, the air will be extracted from the last stage of the compressor, 5% for the NGVs and another 5% for the blades.

## B. Low Pressure Turbine

### 1. Design Criteria

The design procedure for the LPT will be the same as for the HPT, taking into account the parameters and range of values that the authors [1] [18] set for the design of the LPT, which are summarised in Table 28.

**Table 28 LPT Parameters Design Reference**

<b>Exit Nozzle Mach Number</b>	$M < 0.9$
<b>Exit Flow Angle</b>	$-40^\circ < \alpha < 70^\circ$
<b>Exit Rotor Mach Number</b>	$M < 0.9$
<b>Flow Coefficient</b>	$0.5 < \phi < 1.1$
<b>Loading Coefficient</b>	$0.8 < \psi < 2.3$
<b>Degree of reaction</b>	$0.2 < R < 0.7$
<b>Maximum <math>AN^2</math> (RPM<sup>2</sup>in<sup>2</sup>)</b>	$AN^2 < 7E^{10}$
<b>Loss Factor</b>	0.3 – 0.4
<b>Nozzle Axial Aspect Ratio</b>	$1 < AR < 3$
<b>Rotor Axial Aspect Ratio</b>	$3.5 < AR < 7.5$

### 2. Smith Chart and Stages Number

Smith's Chart was also used to determine the efficiency of the LPT. In this case, in the cycle analysis, an isentropic efficiency value of 91% is obtained for the LPT. The Smith Chart for this stage is shown below.

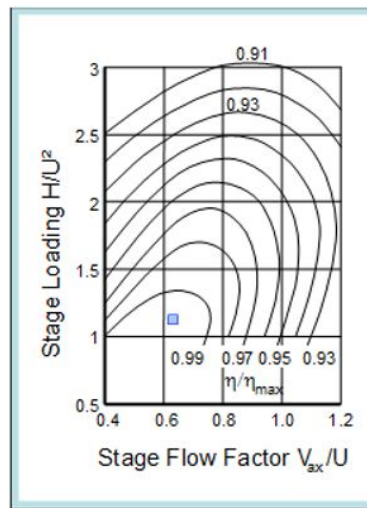


**Fig. 18 LPT Smith Chart**

According to the Figure 18, for an efficiency of 91%, the Stage Flow Factor is 0.63 and the Stage Loading Coefficient is 1.13. Taking into account the workload of the LPT, it was decided to place only one stage, considering that it extracts

enough energy for the engine to meet the operating requirements. A comparison is also made of the values indicated with the reference ranges described in Table 28, showing that they are within the range established by the authors.

### 3. Stage Characteristics

Knowing that the isentropic efficiency of the turbine is 0.91, we proceed to find the other parameters of the stage through GasTurb13, so that the stator and rotor conditions result in the required efficiency. The initial data used to perform the procedure is presented in Table 29.

**Table 29 LPC Input Stage Data**

Property	Value	Unit
<b>LPT Rotor Inlet Dia.</b>	34.23	in
<b>LPT Rotor Exit Dia.</b>	33.49	in
<b>LPT Exit Radius Ratio</b>	0.52	-
<b>LPT Vax.exit/Vax.average</b>	1	-
<b>LPT Loss Factor</b>	0.35	-

For the data above, the following values are obtained as a result, which define the final parameters of the stage.

**Table 30 LPT Output Stage Data**

Property	Value	Unit
<b>LPT Inlet radius ratio</b>	0.62	-
<b>LPT Stator Exit Angle</b>	59.32	deg
<b>LPT Exit Mach Number</b>	0.29	M
<b>LPT Exit Angle</b>	-6.06	deg
<b>LPT Rotor inlet temperature</b>	2393.02	°R
<b>AN<sup>2</sup></b>	5.54E <sup>10</sup>	RPM <sup>2</sup> in <sup>2</sup>
<b>LPT Torque</b>	7430.69	lbft
<b>Design Speed</b>	7120.8	RPM
<b>Number of Blades</b>	69	-
<b>Number of Vanes</b>	66	-
<b>Nozzle Axial Aspect Ratio</b>	1	-
<b>Rotor Axial Aspect Ratio</b>	3.5	-
<b>Pitch/Chord Ratio</b>	0.5	-
<b>LPT exit temperature</b>	2227.09	°R

### 4. Velocity Diagram

After knowing the number of stages and their characteristics, the velocity diagram is plotted, the first triangle corresponds to the stator inlet and the second triangle to the rotor outlet. The Table 31 specifies the velocities values.

**Table 31 LPT Velocity Values**

Property	Value	Unit
<b>Inlet V</b>	1291.44	ft/s
<b>Inlet Vax</b>	658.92	ft/s
<b>Inlet W</b>	662.62	ft/s
<b>Circumferential U</b>	1040.72	ft/s
<b>Exit V</b>	662.62	ft/s
<b>Exit Vax</b>	658.92	ft/s
<b>Exit W</b>	1291.44	ft/s
<b>Stage Loading</b>	1.13	-
<b>Stage Flow Factor</b>	0.63	-

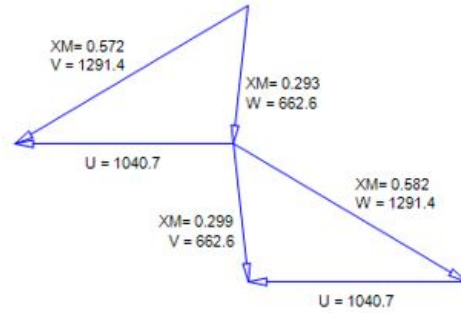


**Fig. 19 LPT Velocity Diagram**

### C. Materials and Manufacturing

The turbine is responsible for generating the energy necessary for the operation of the other components of the engine through the rotation of the blades, for this reason, it is exposed to demanding conditions of temperature and pressure due to the characteristics of the gases leaving the combustion chamber. Therefore, the materials in this section must satisfy the operating requirements to which they will be subjected, such as high creep, fatigue and corrosion resistance at high temperatures [26].

#### 1. Blades Materials

The most commonly used materials for these applications have been nickel superalloys because of their high strength, fracture toughness, resistance to yielding, corrosion and oxidation at elevated temperatures. However, recent research has shown that CMC ceramic matrix composites offer better mechanical and thermal properties at high temperatures with approximately 67% lower weight than nickel superalloys [27]. This type of composite already has a commercial application in the General Electric LEAP engine whose blades were manufactured with Silicon Carbide (SiC) Fiber - Reinforced SiC Matrix (SiC/SiC) [28]. Therefore, it is determined that this material is the best option for the turbine blades, the Table 32 refers to the properties [13].

**Table 32 SiC/SiC Properties. From [13].**

<b>Material Property</b>	<b>Value</b>	<b>Unit</b>
<b>Max. Service Temperature</b>	3370	°R
<b>Thermal Expansion Coefficient</b>	2.22E <sup>-6</sup>	°R <sup>-1</sup>
<b>Density</b>	0.0723	lb/in <sup>3</sup>
<b>Tensile Strength</b>	435	ksi
<b>Young's Modulus</b>	43	Msi

## **8. Mixer Core-Fan Flow**

The forced mixer is responsible for mixing the hot core flow and cold fan flow, generating a more uniform nozzle inlet velocity profile allowing for reduced chemical and acoustic emissions and improved thrust condition during cruise in low bypass engines [29]. Forced mixers can be scalloped or un-scalloped. Wright A. et al. [30], presented an investigation in which they demonstrated that the vortexes of the scalloped lobes develop and dissipate faster in comparison with the un-scalloped lobes presenting less pressure loss at the moment of the mixing of both flows; while Tsui. Y and Wu. P [31] also conducted a numerical investigation based on the finite volume method to study the shape of the trailing edge of the lobes, concluding that the sinusoidal shape with a broad peak region generates a more organized vortex flow, helping to improve the mixing efficiency. The number of lobes also influences this factor, Mundt. Ch and Lieser. J [29] make a comparison between three different numbers of lobes in the BR 710 mixer; the number varies between 16, 18 and 20 with the result that the mixer with 18 lobes performs better during takeoff and the one with 20 lobes helps to improve the SFC at cruise. Regarding mixer pressure, Farokhi [18] establishes a loss of 2%, since the ratio between the fan and core pressures must be close to 1, in this case 0.98 is assumed. For the mixer efficiency, a value of 60% is taken as a reference [32]. After performing the cycle analysis with the above parameters, the mixer must have a diameter of 43.33 inches and a length of 27.45 inches for the engine to meet the thrust requirements. A component characteristic summary is given in Table 33.

**Table 33 Mixer Values**

<b>Parameter</b>	<b>Value</b>	<b>Unit</b>
<b>Type</b>	Scalloped	-
<b>Lobes form</b>	Sinusoidal	-
<b>Number of lobes</b>	20	-
<b>Lobe angular spacing</b>	18	deg
<b>Efficiency</b>	60	%
<b>Pressure Loss</b>	2	%
<b>Pressure Ratio</b>	0.98	-
<b>Length</b>	27.45	in
<b>Diameter</b>	43.33	in

## 9. Nozzle

### A. Inlet Conditions

To configure and design a properly engine nozzle, it is required to know the inlet nozzle conditions and environment. This essential data allows the establishment of design points, which permit to clarify which nozzle configuration and number of stages could be adopted. Parameters of on design and off design inlet condition are shown below in Table 34.

**Table 34 Nozzle inlet conditions**

<b>On Design</b>		<b>Off Design</b>	
<b>Parameter</b>	<b>Value</b>	<b>Parameter</b>	<b>Value</b>
<b>MassFlow [lbm/s]</b>	286.70	<b>MassFlow [lbm/s]</b>	475.60
<b>Total Temperature [°R]</b>	1596.09	<b>Total Temperature [°R]</b>	1999.17
<b>Static Temperature [°R]</b>	1529.07	<b>Static Temperature [°R]</b>	1923.08
<b>Total Pressure [psia]</b>	21.53	<b>Total Pressure [psia]</b>	47.48
<b>Static Pressure [psia]</b>	11.32	<b>Static Pressure [psia]</b>	40.40
<b>Velocity [ft/s]</b>	1776.25	<b>Velocity [ft/s]</b>	1042.73
<b>Area [in<sup>2</sup>]</b>	1350.7	<b>Area [in<sup>2</sup>]</b>	1158.21
<b>Mach Number</b>	0.50	<b>Mach Number</b>	0.49

### B. Design Geometry and Area Scheduling

JULIO engine requires a specific control around the exhaust area regarding the flight development. The throat must be able to be a back-pressure controller of flow coming from the low-pressure turbine, allowing a wide range of operation of different geometries [18]. In this case, a divergent section will be a variable area as the last component of the nozzle, more precisely how it is shown in the image below.

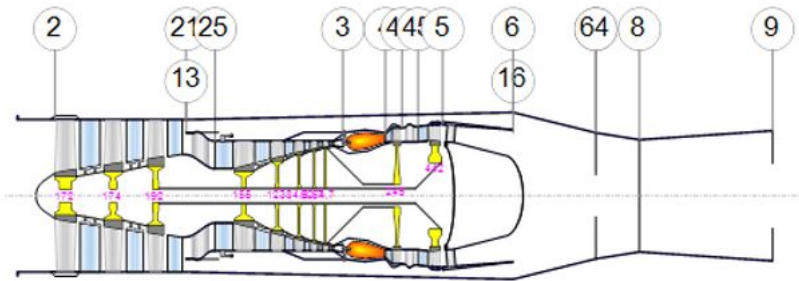


**Fig. 20 Engine Overall Geometry.**

Between the 8 and 9 section lays the divergent variable area that consist of one stage.

After establishing the type of nozzle that the engine will have, it's necessary to calculate the dimensions for cruise and takeoff, so that the FADEC system is programmed to accommodate the section from 8 to 9 to the dimensions that are required. For the sizing of the nozzle, the methodology of Mattingly's book [1] based on the design of a convergent-divergent nozzle is used. The nozzle is calculated in the On Design condition of Mach 2.0 at 53000 feet, and in Off Design at mach 0.3 and sea level. The results of the nozzle design are given in the Table 36 and the values of the final nozzle geometry are in Table 35.

**Table 35 Nozzle Geometry Values**

Parameter	On Design	Off Design	Unit
<b>Primary Half Angle (<math>\theta</math>)</b>	8.95	9.37	deg
<b>Secondary Half Angle (<math>\alpha</math>)</b>	3.45	3.85	deg
<b>Convergent Section Length</b>	14.51	13.44	in
<b>Divergent Section Length</b>	44.27	40.75	in
<b>Nozzle Throat Radius</b>	18.15	16.71	in
<b>Nozzle Exit Radius</b>	21.09	17.86	in

The nozzle purpose is to increase thrust, however, depending on the regime, the divergent zone will either increase or reduce the area. For cruise, the engine is in supersonic regime, so increasing the area helps the flow to accelerate. In the takeoff it is in a subsonic regime so the nozzle must decrease the exit area to achieve a lower static pressure and accelerate the flow. However, this will have the noise implication in this flight phase, which will be discussed in the next subsection.

**Table 36 Nozzle Design Results**

<b>Parameter</b>	<b>Cruise</b>	<b>takeoff</b>
<b>Area Ratio A9/A8</b>	1.35	1.14
<b>Throat Area A8 (ft<sup>2</sup>)</b>	7.19	6.09
<b>Pt8 [psi]</b>	21.10	46.53
<b>Tt8 [R]</b>	1596.09	1999.17
<b>MFP [33]</b>	0.54	0.54
<b>m point 8 [lb/s]</b>	286.71	475.60
<b>Effective Throat Area A8e (ft<sup>2</sup>)</b>	6.93	5.84
<b>Nozzle Exit Area A9 (ft<sup>2</sup>)</b>	9.70	6.96
<b>Discharge Coefficient Cd</b>	0.99	0.99
<b>V9 [ft/s]</b>	2669.94	2656.60
<b>A/A*</b>	1.36	1.15
<b>Ideal Exit Mach Number M9i (using A/A* sup in [33] )</b>	1.70	1.44
<b>P9i/Pt9i (using A/A* sup in [33])</b>	0.21	0.30
<b>P9i [psi]</b>	4.35	13.96
<b>V9i</b>	2677.74	2675.28
<b>P9</b>	4.33	14.25
<b>Pt9</b>	21.10	46.53
<b>Nozzle Gross Thrust Coefficient Cfg</b>	0.94	0.99
<b>Velocity Coefficient Cv</b>	1.00	0.99
<b>Actual Nozzle Gross Thrust Fg (lbf)</b>	10011.34	33609.48
<b>Ideal Nozzle Gross Thrust Fgi (lbf)</b>	10040.57	33845.77
<b>Actual Exit Mach Number (M<sub>9</sub>)</b>	1.69	1.43
<b>Ambient Pressure P0 (psi)</b>	1.45	14.69
<b>Nozzle Exit Pressure P9 (psi)</b>	4.32	14.25

### **C. Engine Noise Attenuation**

One of the requirements for the engine design established by the RFP is that the exhaust gas velocity during the takeoff phase has a maximum value of 1150 ft/s [8]. This is consider a main factor because the causes of noise pollution near the airports. For this design it is proposed to use a mixer ejector before the convergent zone and Chevrons at the end of the nozzle duct.

#### *1. Mixer Ejector*

The mixer ejector introduces high pressure ambient air into the engine (blue arrows in Figure 24). Initially, the internal fluid (red arrows) and the incoming fluid (blue arrows) remain separated due to the shear force between the streams, but as the two flows move through the nozzle, they mix, increasing the mass flow and reducing the velocity of the gases exiting the nozzle due to the transfer of kinetic energy between the core flow and the incoming air mass

[Hunter]. In addition, this system helps to increase the mass flow keeping the thrust produced by the nozzle [5]. Figure 21 shows the the mixer ejector configuration in cruise and takeoff.

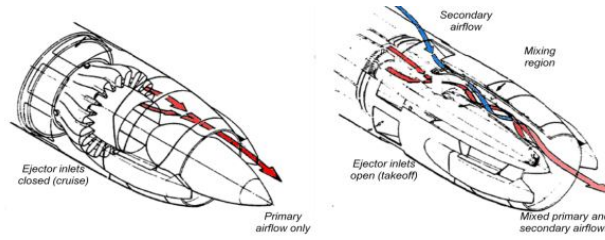


**Fig. 21 JT8D-17 20-lobe ejector nozzle showing cruise (left) and takeoff (right) operation. From [5]**

To estimate the increase in airflow necessary to reduce the velocity from 2656 ft/s to 1150 ft/s, the methodology presented in [5] and [6] is adopted, based on relating the percentage decrease in velocity to the percentage of Mass Flow Augmentation MFA, whose value is the ratio between the amount of additional ambient air and the unincreased exhaust mass flow. Figure 22 illustrates the graph relating the MFA to the velocity percentage reduction.

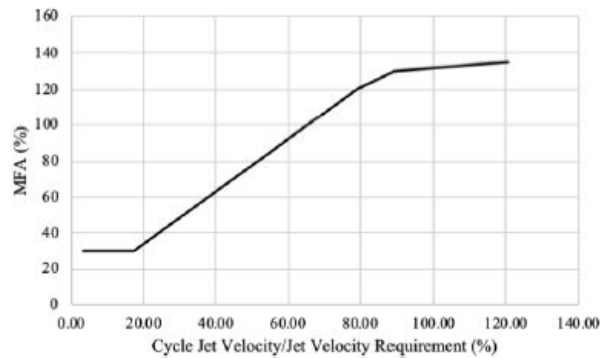


**Fig. 22 Mixer Ejector Model. From [6].**

Taking into account that to achieve a value of 1150 ft/s a 57% reduction in the outflow velocity of the gases is needed, according to the graph the MFA is 90%, the value of the mass flow without taking into account the increase of air is 475.61 lb/s, therefore, the amount of additional air must be 428.05 lb/s to reach the velocity required by the RFP.

## 2. Chevrons

Nowadays a noise suppression system is required in modern aircraft, especially when talking about supersonic vehicles. Different bibliography agrees that noise issues could be reduced as the exhaust speed is reduced too [18]. In this case, there is no interest on change the engine speed, rather it has been opted to implement a Chevron nozzle.

Chevrons are small splines located at the end of the exhaust. They may not be too deep, otherwise the engine may experience loss of thrust [18]. The JULIO engine will incorporate small serrations to avoid loss of thrust, using a 3I12C24 configuration that reaches a noise suppression benefit of 2.71 EPN dB. This condition will let the engine have a loss in thrust coefficient less than 1% at cruise level and will allow noise reduction in all flight conditions [7].

Configuration	Noise benefit EPNdB	%Loss in thrust coefficient at cruise
3C12B	1.36	0.55
3I12B	2.18	0.32
3I12C24	2.71	0.06
3T24B	2.37	0.99
3T48B	2.09	0.77
3T24C24	—	0.43
3T48C24	—	0.51
3A12B	—	0.34
3A12C24	—	0.49

**Fig. 23 Noise Benefit and Cruise Thrust Loss Data. From [7].**

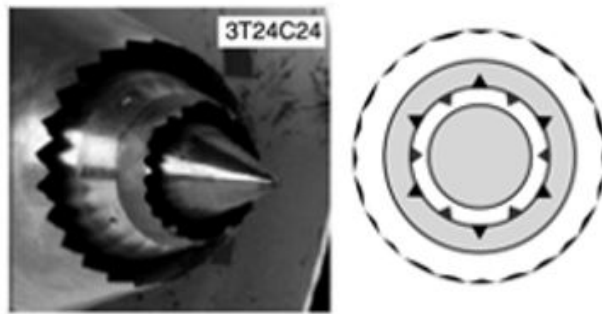


**Fig. 24 Chevron 3T24C24 Configuration. From [7].**

## 10. Shaft

JULIO will be designed with two shafts, consisting of two independent turbines since the main advantage of this system is that the compressor and the turbine are driven at the optimum speed for the power for which they have been designed. This speed was optimized and conditioned to the specific requirements of the engine [34].

For this engine JULIO, the shaft will be designed so that in the cruise stage, which is where it will remain most of the time, the balance is equal to 0 so that the shaft does not suffer tension or compression efforts.

The important thing that in this motor design the shaft and the bearings have easy access without having to disassemble everything else, the bearings must not only transmit the resulting forces of the internal forces of the compressor and turbine components but also can absorb contraction or expansion according to the temperatures they provide [35].

Particularly for this case, JULIO was designed with rotation speeds of the low shaft (Fan - low turbine) for 7120.84 rpm and the high shaft (high compressor - high turbine) for 10 097.76 rpm, speeds that are optimal to meet the requirements of this engine.

## **11. Engine Subsystems**

### **A. Anti – Icing**

The anti-icing system in turbofan engines is used in two specific areas at the air inlet, are the rotor fan and in the inlet lip. The anti-icing system of the JULIO engine works employing the engine bleed air at a temperature of 900 K, which is obtained from the first stage of the HPC. Therefore, it is crucial to consider this subsystem because the aircraft flies in cruising conditions at an altitude of 53000 ft, a speed Mach 2 and a temperature of 236.65 K with ISA +5, close to the freezing point, since this ice formation can lead to engine damage. [36]

### **B. Bleed Air System**

This system is responsible for supplying air for different purposes within the operation of the aircraft, such as feeding the pneumatic system [37] .

For this case, in our engine JULIO, this air is extracted directly from the engine compressor and extracted directly from the engine, from the HPC for different uses since the temperature and pressure required to vary according to its use [36], for example, we can supply a requirement 3 lb/s for air conditioning.

This air is also used for other processes within the aircraft such as engine ignition, the anti-ice system, cabin pressurization, among others, which guarantees a correct operation of this system within our engine JULIO.

### **C. Engine Control System**

It is an electronic control system on which the pilot has no impact, it is designed in a redundant way that allows high reliability, statistically much higher than traditional systems. A FADEC system is characterized by being autonomous, self-monitoring, self-operated and at the same time redundant.

This system provides automatic monitoring of engine performance, significantly reducing pilot workload by constantly monitoring parameters such as engine Over-speed and supercharging. [38].

For this case, we will use a FADEC from the supplier BAE Systems, since from the experience acquired by this

supplier we can see how they have acted correctly in equipment such as the f22, the Boeing 777, and the Airbus A380.

This FADEC will mainly be in charge of eliminating the possibility of exceeding any engine limitation, likewise, it will deliver a real-time diagnosis of the state of the engine cycle and will control parameters such as fuel flow, stator vane position, and bleed valve position. In addition, this system will control the ignition and restart of the engine to provide optimum efficiency and keep the engine in good condition, with input parameters such as air density, throttle position, engine pressure and temperature, and many other parameters which are analyzed by the ECC (Electronic Engine Control) around 70 times per second [39].

This BAE Systems FADEC will also feature a redundant system, it has been certified by the vendor to provide full operational capability in the event of a partial system failure. What it will provide provides high fuel efficiency as most engine performance parameters are controlled by it.

#### **D. Starting System**

It is important to clarify that the starting system is always linked to the ignition system, these systems always work together, but for general purposes, they are described independently. These systems are normally of the pneumatic type since it represents very little weight within the total components of the engine compared to an electrical system, for this reason, it is then linked to the bleed air system. Engines are normally started with two generators in each of the engines called starter generators.

The JULIO engine starting sequence begins with the acceleration of the “HP spool”, generates a flow of air through the combustion chamber, and allows the fuel / air mixture to be flammable [36]. In our case, once the shaft has a safe speed (approximately 20%) a pressure valve called (shut off valve) opens and the fuel flows to the fuel nozzle; The ignition procedure will occur when the fuel reaches the combustion chamber, after the combustion process the EGT temperature will begin to rise.

The JULIO starting system will have the following components: connection of the starter motor to the pneumatic system, start control, star valve (to shut off the air supply) and cabin indicator controls.

#### **E. Lubrication System**

The lubrication system for this case will provide proper lubrication and cooling for all gears, bearings, and splines, as it will have the ability to collect debris that could produce a failure due to accumulation or friction with these parts.

In addition, this system will have the ability within the engine to protect components that are in contact with the lubricant around corrosion [36]. For this purpose, in this case, it will have a spring-loaded relief valve that will allow the oil to be returned directly to the pressure pump when the limit or maximum design value is exceeded and provides a constant supply at the normal operating speeds of the engine.

## References

- [1] Mattingly, J., Heiser, W., and Pratt, D., *Aircraft Engine Design, Second Edition*, AIAA Education Series, 2002.
- [2] Lefebvre, A. H., and Ballal, D. R., *Gas Turbine Combustion, Third Edition*, CRC press, 2010.
- [3] Farokhi, S., *Aircraft propulsion*, John Wiley & Sons, 2014.
- [4] ICAO, "Aircraft Engine Emissions Databank," url<https://www.easa.europa.eu/eaer/topics/technology-and-design/aircraft-engine-emissions>, 2018.
- [5] Hendricks, . S. J., E., *A Multidisciplinary Approach to Mixer-Ejector Analysis and Design.*, 48th AIAA/ASME/SAE/ASEE Joint Propulsion Conference Exhibit. doi:10.2514/6.2012-4224, 2012.
- [6] Vlady, T., Ong, S. K., Kemplay, O., and Zakharov, S., *YJ-2030: Candidate Engine for a Supersonic Business Jet*, Georgia Institute of Technology, 2020.
- [7] Zaman, K., "Evolution from tabs to chevron technology - A review," *NASA Glenn Research Center*, Vol. 10, No. 5, 2011, pp. 685–710.
- [8] Halliwell, I., *Let's Re-Engine the Concorde!*, American Institute of Aeronautics and Astronautics - AIAA, 2020.
- [9] ConcordeSt., "Concorde: Technical Specs." , 2021. URL <http://www.concordest.com/powerplant.html>.
- [10] Bose, T., *Airbreathing propulsion*, Springer, 2012.
- [11] Gasturb GmbH, "Gasturb Software for Aircraft Engines," , 2020.
- [12] Materials, A., "'Super Alloy Nimonic Alloy 263<sup>tm</sup>,'" , 2021. URL <https://www.azom.com/article.aspx?ArticleID=7667>.
- [13] Zinkle, S. L., S.J, *Thermophysical and Mechanical Properties of SiC/SiC Composites.*, Oak Ridge National Laboratory., 1998.
- [14] Naumenko, A., "'What are the differences between a mixed and an unmixed turbofan?'" , 2020. URL <https://www.quora.com/What-are-the-differences-between-a-mixed-and-an-unmixed-turbofan>.
- [15] Aircraft Engineering, "Concorde's Olympus 593: The British centrepiece at the Peking exhibition," *Aircraft Engineering and Aerospace Technology*, Vol. 45, No. 3, 1973, pp. 6–8.
- [16] Rettie, I. H., and Lewis, W. G., "Design and Development of of an Air Intake for a Supersonic Transport Aircraft," *Journal of Aircraft*, Vol. 5, No. 5, 1968, pp. 513–521.

- [17] Saravanamuttoo, H., Rogers, G., Cohen, H., Straznicki, P., and Nix, A., *Gas Turbine Theory, Seventh Edition*, Pearson Education, 2017.
- [18] Farokhi, S., *Aircraft Propulsion, Second Edition*, Wiley & Sons Ltd, 2014.
- [19] Liu, Y., Sun, X., Sethi, V., Nalianda, D., Li, Y.-G., and Wang, L., “Review of modern low emissions combustion technologies for aero gas turbine engines,” *Progress in Aerospace Sciences*, Vol. 94, 2017, pp. 12–45. <https://doi.org/https://doi.org/10.1016/j.paerosci.2017.08.001>, URL <https://www.sciencedirect.com/science/article/pii/S037604211630118X>.
- [20] Ren, X., Xue, X., Brady, K. B., Sung, C.-J., and Mongia, H. C., “Fundamental investigations for lowering emissions and improving operability,” *Propulsion and Power Research*, Vol. 7, No. 3, 2018, pp. 197–204. <https://doi.org/https://doi.org/10.1016/j.jprr.2018.07.001>, URL <https://www.sciencedirect.com/science/article/pii/S2212540X18300373>.
- [21] Ommi, F., and Azimi, M., “Most effective combustion technologies for reducing Nox emissions in aero gas turbines,” *The International Journal of Multiphysics*, Vol. 6, 2012, pp. 417–424. <https://doi.org/10.1260/1750-9548.6.4.417>.
- [22] Rolls-Royce, *The Jet Engine*, Rolls-Royce plc, ISBN 0902121 235, 1986.
- [23] Team, D., Yingjun, W., Mingha, G., and Yu, H., “Signature Page,” 2020.
- [24] Epfl.ch, ““Turbine Blade Cooling”,”, 2020. URL <https://www.epfl.ch/labs/gtt/page-63154-fr-html/page-63560-fr-html/page-63563-fr-html/>.
- [25] Technology.nasa.gov, ““Patent Details”,”, 2020. URL <https://technology.nasa.gov/patent/LEW-TOPS-52>.
- [26] OKURA, T., *Materials for aircraft engine*, Colorado University, 2015.
- [27] Muktinutalapati, N. R., *Materials for Gas Turbines – An Overview, Advances in Gas Turbine Technology*, VIT University, 2011.
- [28] Ceramics.org, ““Emerging Ceramics and Glass Techonology”,”, 2019. URL <http://ceramics.org/wp-content/bulletin/2019/pdf/April2019.pdf>.
- [29] Mundt, C., and Lieser, J., *Performance improvement of propulsion systems by optimization of the mixing efficiency and pressure loss of forced mixers.*, European Propulsion Forum., 2001.
- [30] Wright, A., Lei, Z., Mahallati, A., Cunningham, M., and Militzer, J., “Effects of Scaloping on the Mixing Mechanisms of Forced Mixers With Highly Swirling Core Flow,” *Journal of Engineering for Gas Turbines and Power*, Vol. 135, 2013, pp. 071202–071202. <https://doi.org/10.1115/1.4024043>.

- [31] Tsui, Y.-Y., "EFFECTS OF LOBE GEOMETRY ON THE MIXING FLOW IN MULTILOBE MIXERS," *Numerical Heat Transfer, Part A: Applications*, Vol. 39, 2001, pp. 61–77. <https://doi.org/10.1080/10407780121487>.
- [32] Bjorn Cleton, E. A., *Effect of mixing Mach number and mixing efficiency on the preliminary cycle design of mixed high-BPR turbofans.*, Propulsion Engineering Centre, Cranfield University, 2019.
- [33] Dept.aoe.vt.edu, "'Compressible Aerodynamics Calculator'," , 2021. URL <http://www.dept.aoe.vt.edu/~devenpor/aoe3114/calc.html>.
- [34] Hamburg, G., "Thermal Engineering," *Equipment for Engineering Education*, Vol. 3, No. n.d., n.d., p. 143.
- [35] Parsons, D., "Industry ak US Army, one shaft or two for new helicopter engine," *flight global*, Vol. n.d., No. n.d., 2015, p. n.d.
- [36] Diesinger, A. L., *Systems of Commercial Turbofan Engine!*, Springer-Verlang Berlin Heidelberg, 2008.
- [37] Skybrary, "Aircraft Bleed Air system," *skybrary*, Vol. n.d., No. n.d., 2019, p. 2.
- [38] Administration, F. A., "14 CFR 33.28," *Advisory Circular*, Vol. 1, No. 33.28-1, 2001, pp. 1–3.
- [39] FAA Safety Brief, "Full Authority Digital Engine Control (FADEC)," , 2017.